Journal of Neuroinflammation

RESEARCH

Open Access

Rescue of in vitro models of CSF1R-related adult-onset leukodystrophy by iluzanebart: mechanisms and therapeutic implications of TREM2 agonism

Kelley C. Larson[1*], Frederick W. Gergits[1], Abigail J. Renoux[1], Elizabeth J. Weisman[1], Borislav Dejanovic[1], Liyue Huang[1], Bhaumik Pandya[1], Donald G. McLaren[1], Berkley A. Lynch[2], Richard Fisher[3], Evan Thackaberry[1], David Gray[1], Francois Gaudreault[1] and Christian Mirescu[1]

Abstract

Microglia dysfunction is implicated in several neurodegenerative disorders, including a rare microgliopathy; CSF1R-related adult-onset leukoencephalopathy with axonal spheroids and pigmented glia (CSF1R-ALSP). CSF1R-ALSP is caused by heterozygous loss-of-function mutations in the colony stimulating factor 1 receptor (CSF1R) gene, which encodes a receptor required for the differentiation of myeloid cells, as well as for microglial survival and proliferation. Similar functions have also been ascribed to triggering receptor expressed on myeloid cells 2 (TREM2), which shares an analogous microglia enrichment profile and converging intracellular signaling pathway mediated by spleen associated tyrosine kinase (SYK) and phosphoinositide-3-kinase (PI3K). Iluzanebart is a human monoclonal IgG1, human TREM2 (hTREM2) agonist antibody under development for the treatment of CSF1R-ALSP. To explore the therapeutic hypothesis that loss of CSF1R signaling and related microglial hypofunction can be circumvented via activation of TREM2, we evaluated the potential of iluzanebart to compensate for CSF1R loss-of-function. Herein, we demonstrate that iluzanebart is a potent, dose-dependent, and specific activator of TREM2 signaling in human primary cells. Iluzanebart treatment rescued viability of human monocyte-derived macrophages (hMDM) and induced pluripotent stem cell-derived human microglia (iMGL) in multiple in vitro models of CSF1R-ALSP, including in induced pluripotent stem cell (iPSC) differentiated microglia carrying the heterozygous I794T mutation found in CSF1R-ALSP patients. Additionally, iluzanebart treatment in microglia modulated surface levels of CSF1R, resulting in increased receptor activation as measured by phosphorylation of CSF1R. Differentially expressed genes identified in the hippocampus of mice treated with iluzanebart were exemplary of TREM2 activation and were related to cell proliferation, regulation of inflammatory processes, and innate immune response pathways. Proliferation of microglia, changes in protein levels of specific chemokines identified by gene expression analysis, and increased CSF1R levels were also confirmed in vivo. These findings demonstrate that iluzanebart is a potent and selective TREM2 agonistic antibody, with pharmacology that supports the hypothesis that TREM2 activation can compensate for CSF1R dysfunction and its continued clinical development for individuals with CSF1R-ALSP.

*Correspondence:
Kelley C. Larson
klarson@vigilneuro.com
Full list of author information is available at the end of the article

Introduction

CSF1R-related adult-onset leukodystrophy with axonal spheroids and pigmented glia (CSF1R-ALSP), is an inherited, autosomal dominant, and often lethal disorder caused by loss of function mutations in the CSF1R gene, resulting in hypofunction, dysregulation, and apoptosis of microglia. A rare neurological disorder, CSF1R-ALSP is neuropathologically characterized by the presence of demyelination, swollen axons, and pigmented glial cells, which lead to adult-onset, rapidly progressing neurological symptoms typically presenting in the 4th decade of life [1, 2]. Recent research involving the UK BioBank, a population-scale whole-exome sequencing data set from the United Kingdom, shows the frequency of pathogenic and likely pathogenic CSF1R variants to be 281 per million [3]. This data implies that CSF1R-ALSP may be more prevalent than would be expected based on the number of CSF1R-ALSP cases documented in the literature, possibly due to its high rate of initial misdiagnosis [4], as CSF1R-ALSP patients are frequently misdiagnosed with more common neurological diseases including multiple sclerosis and Alzheimer's disease [5]. Furthermore, there are no approved therapies for CSF1R-ALSP; the current standard of care seeks to alleviate the motor and sensory symptoms that stem from the disease and attempts to minimize the decline in quality of life [5]. The development of disease-modifying therapeutics for CSF1R-ALSP remains a significant and critical unmet need.

CSF1R-ALSP is caused by heterozygous loss of function mutations in the CSF1R gene, resulting in impaired receptor function and diminished downstream signaling [6, 7]. Most mutations in CSF1R that are associated with CSF1R-ALSP have been identified in the tyrosine kinase domains, including the most frequently observed mutation, I794T, described herein. These mutations result in the disruption of the ability of the kinase domains to auto-phosphorylate, resulting in the subsequent loss of downstream CSF1R signaling. In the CNS, CSF1R regulates critical functions of myeloid cells, which include microglia, monocytes, and macrophages, and disturbances in these critical functions are implicated in the pathophysiology of CSF1R-ALSP [8, 9]. The binding of CSF1R ligands, CSF1 or IL34, regulate microglia survival, differentiation, and phagocytic activity, and therefore plays a key role in maintaining homeostasis of the central nervous system (CNS) [10]. In addition to survival and proliferation of microglia in the adult brain, CSF1R signaling is critical for the generation of microglia from progenitor cells during development. This is highlighted by the fact that homozygous CSF1R knockout mice show an almost complete loss of microglia in the parenchyma [11]. Analysis of postmortem brain tissue from individuals with CSF1R-ALSP has also demonstrated that loss of CSF1R function leads to a reduction in microglial numbers, as well as a loss of homeostatic phenotypes in the surviving microglia. These surviving microglia demonstrate an abnormal tissue distribution, altered morphology, and increased inflammatory phenotype, which likely contributes to the loss of white matter and changes in ventricular volume observed in CSF1R-ALSP [12–14].

The microglia-enriched triggering receptor expressed on myeloid cells 2 (TREM2) is an environmental sensor that engages a broad range of endogenous substrates, including phospholipids associated with myelin and cellular debris, as well as neurodegenerative disease-associated lipoproteins such as ApoE and LDL [15]. Activation of TREM2 receptors results in a coordinated intracellular response to the diseased extracellular microenvironment leading to changes in microglia that foster the resolution of tissue damage and restoration of homeostasis [16]. The critical importance of TREM2 in brain homeostasis is best exemplified by the fact that homozygous loss of function mutations in TREM2 result in a devastating progressive dementia, Nasu-Hakola Disease, which is usually fatal by the 5th decade of life [17]. In mice, TREM2 has been demonstrated to play a fundamental role in the ability of microglia to transition from a homeostatic state to a restorative, neuroprotective state (known as disease associated microglia, or DAM) in response to damage-associated molecular patterns (DAMPs) caused by cellular debris, degraded myelin, or amyloid-beta deposits [18]. Similar to CSF1R, TREM2 expression and activation has been shown to promote microglial survival and proliferation [19, 20]. This critical role for TREM2 in brain health and resilience is critically supported by human genetic TREM2 variants that are associated with increased risk for neurodegenerative diseases [21, 22].

While TREM2 signaling is entirely dependent on recruitment and phosphorylation of its adaptor proteins DAP12 or DAP10, CSF1R can also selectively signal through DAP12 [23], leading to a cascade of phosphorylation events that result in the communication of pro-survival signals to the cell [24, 25]. Therefore, it is hypothesized that loss of function of CSF1R, resulting in reduced signaling through SYK and PI3K [26] could be counteracted via agonism of the TREM2 receptor, leading to compensatory phosphorylation and pathway activation. The present study evaluates the potency of iluzanebart as an activator of TREM2 receptor signaling in multiple in vitro models of CSF1R-ALSP, and in three independent cell types: HEK293T cells genetically modified to express human TREM2 and DAP12 (hTREM2-HEK293T), human monocyte-derived macrophages (hMDM), and induced pluripotent stem cell-derived human microglia (iMGL). Due to the lack of in vivo models that faithfully recapitulate the pathophysiology

of CSF1R-ALSP, these studies focus on rescue of phenotypes in human in vitro models. Herein we detail the pharmacodynamic effects of iluzanebart on CSF1R signaling deficiency in multiple cell lines and present results from preliminary in vivo pharmacokinetic/pharmacodynamic experiments of iluzanebart treatment in mice.

Results

Iluzanebart is a potent activator of TREM2 across multiple cell-based model systems

Binding of iluzanebart to the human TREM2 receptor has been epitope mapped to the extracellular Ig-like domain of TREM2, with an average Kd of 1.25 nM (Supplemental Figs. 1 and 2). The cell-based potency of iluzanebart as an agonist of TREM2 was evaluated in HEK293T cells engineered to express both human TREM2 (hTREM2) and human DAP12 (hDAP12). Phosphorylation of both DAP12 and SYK serve as indicators of TREM2 receptor activation, and SYK activation is used as a surrogate measurement for downstream pathway signaling [16]. Levels of both pSYK and pDAP12 were measured following treatment with iluzanebart at a range of concentrations (Fig. 1A and B). Compared to its IgG control, which showed no ability to stimulate SYK phosphorylation, iluzanebart was found to have an average EC50 of 0.27 nM. The high potency of iluzanebart to activate TREM2 signaling was confirmed when activation was measured by pDAP12, which resulted in an average EC50 of 1.14 nM.

To determine if iluzanebart's ability to activate TREM2 would be maintained in relevant human primary cells, it was next assessed in a human monocyte-derived macrophage (hMDM) cell culture system. Compared to its IgG control, which showed no ability to stimulate phosphorylation of SYK, iluzanebart was found to have

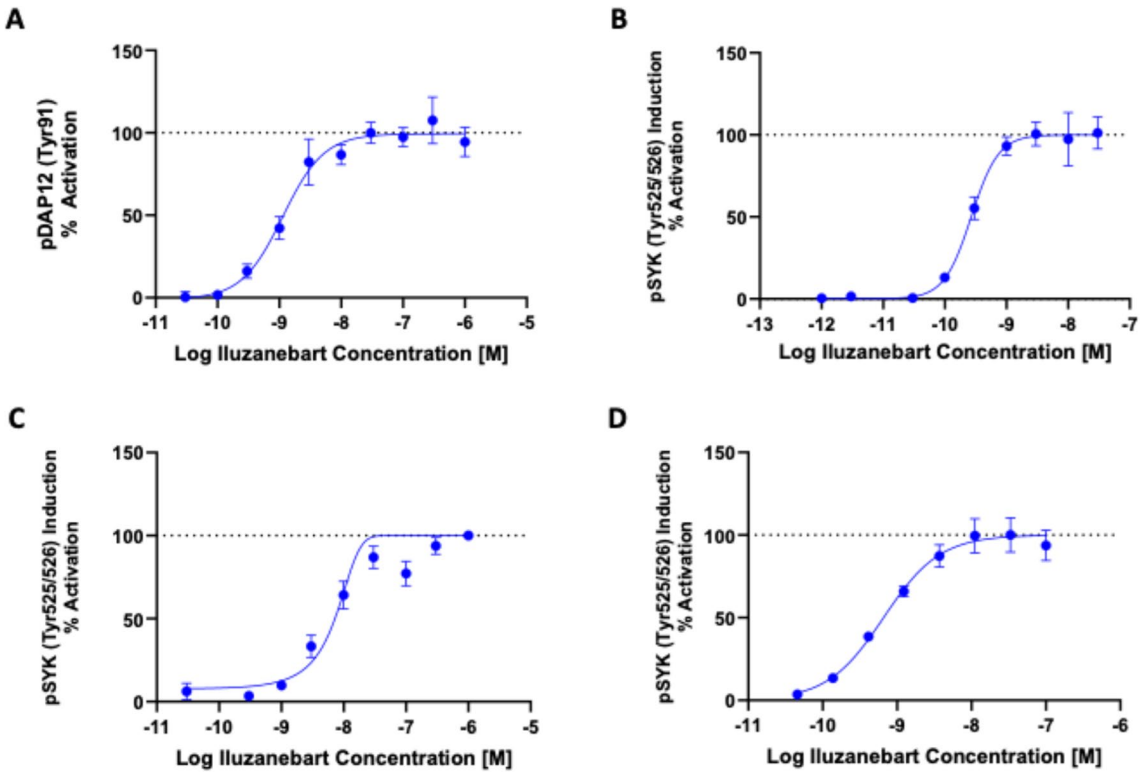

Fig. 1 Potency of iluzanebart across in vitro human model systems. Activation of TREM2 via protein phosphorylation was assessed using AlphaLISA assays. **A HEK-hTREM2 Cells.** In HEK293T cells expressing human TREM2 and DAP12, pDAP12 in response to iluzanebart for 45 min was analyzed, resulting in an EC50 potency of 1.09 nM (n = 2 independent experiments). Results are shown as normalized to IgG control, which did not stimulate SYK phosphorylation, and reported as % of maximal activation. **B HEK-hTREM2 Cells.** Similarly, in the same HEK293T cell line, iluzanebart had a potency of 0.19 nM (n = 3 independent experiments) when measuring phosphorylation of SYK. Results are shown as normalized to IgG control, which did not stimulate SYK phosphorylation, and reported as % of maximal activation. **C Human Monocyte Derived Macrophages (hMDM).** In human MDM cells, treatment with iluzanebart for 45 min stimulated phosphorylation of SYK with an average EC50 potency of 4.77 nM (n = 4 independent experiments). Results are shown as normalized to IgG control, which did not stimulate SYK phosphorylation, and reported as % of maximal activation. **D iPSC Derived Human Microglia (iMGL)**. In human iPSC-derived microglia cells, iluzanebart treatment for 5 min stimulated phosphorylation of SYK with an average EC50 potency of 0.63 nM (n = 6 independent experiments), and is shown as normalized to IgG control, which did not stimulate SYK phosphorylation, and reported as % of maximal activation

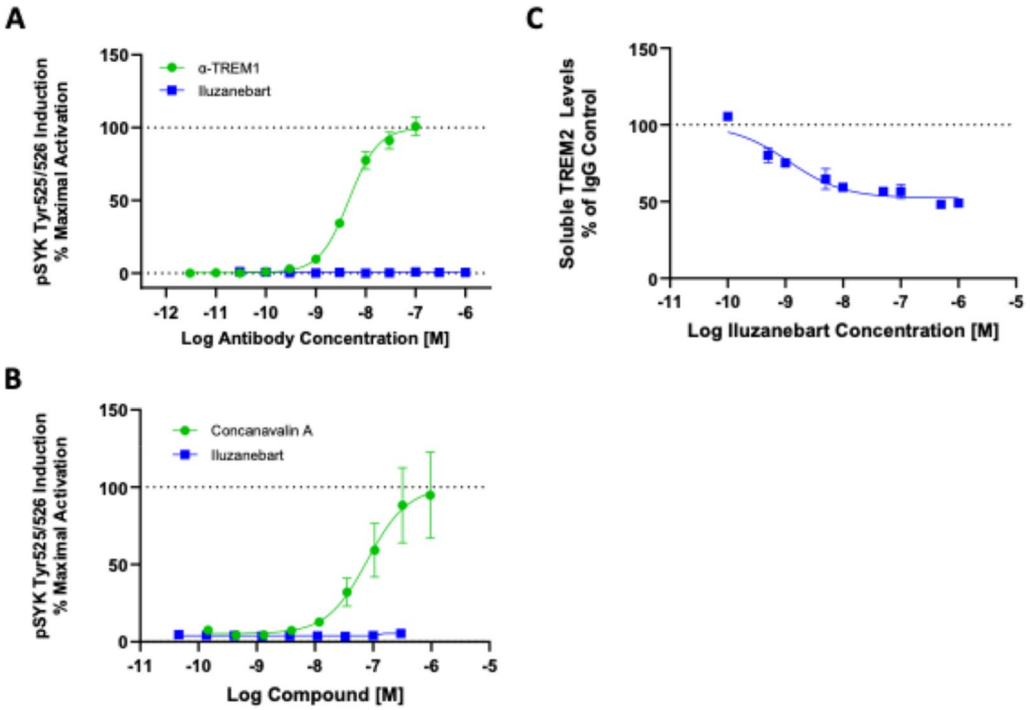

Fig. 2 Iluzanebart is a specific agonist of human TREM2. **A hTREM1-HEK.** In a HEK293T cell line expressing hTREM1 and hDAP12, an anti-TREM1 antibody (green) stimulated phosphorylation of SYK after 45-min treatment, whereas iluzanebart (blue) did not (n = 3 independent experiments), confirming that iluzanebart is a TREM2-specific agonist with no cross-reactivity to the related TREM1 receptor. **B TREM2 -/- iMGL.** Iluzanebart (blue) does not stimulate pSYK in TREM2$^{-/-}$ human iPSC-derived microglia. Concanavalin A (green) was used as a positive control demonstrating that TREM2$^{-/-}$ cells can activate pSYK in response to TREM2-independent activators. Data shown is normalized to IgG control after 5 min exposure (n = 2 independent experiments) and reported as % of maximal activation. **C iPSC Derived Human iMGL.** Treatment of human iPSC microglia with iluzanebart reduced levels of soluble TREM2 levels after 24 h, compared to IgG control which had no effect (n = 2 independent experiments)

an average EC50 of 4.77 nM in hMDM cells (Fig. 1C). Finally, iluzanebart potency was assessed in human induced pluripotent stem cell (iPSC)-derived microglia cells (iMGL) and was found to have an average EC50 of 0.63 nM, while treatment with its IgG control induced no phosphorylation of SYK (Fig. 1D). While potencies may be affected by differences in the levels of TREM2 receptor at the cell surface among the various cell types tested, overall, these data show that iluzanebart is a potent, subnanomolar agonist of human TREM2.

Iluzanebart is a specific agonist of human TREM2

Phosphorylation of SYK is not TREM2 specific; phosphorylation of SYK can also be induced through activation of TREM1, another member of the TREM family of receptors, but one that is genetically distinct from TREM2. To determine whether iluzanebart exhibits off-target effects through TREM1, or is specific to TREM2, HEK293T cells engineered to express human TREM1 (but not hTREM2) and human DAP12 were treated with iluzanebart. While a positive control human anti-TREM1 antibody stimulated SYK phosphorylation as expected, iluzanebart was unable to stimulate SYK phosphorylation in cells expressing TREM1 (Fig. 2A). Therefore, activation of SYK phosphorylation by iluzanebart is TREM2 specific.

Iluzanebart specificity for TREM2 was further confirmed in human microglia using TREM2 knockout (TREM2 -/-) iMGL. As shown in Fig. 2C, iluzanebart was unable to activate SYK in TREM2$^{-/-}$ cells (Fig. 2B). Concanavalin A, which activates SYK through a TREM-independent mechanism [27], was used as a positive control. Activation of SYK by Concanavalin A confirmed that SYK was capable of being phosphorylated in this system, even in the absence of TREM2. Together, these data suggest that iluzanebart is a specific, potent agonist of TREM2.

TREM2 undergoes regular proteolytic processing by cleavage and subsequent shedding of its extracellular ectodomain, producing soluble TREM2 (sTREM2) [28–30]. Recent studies have correlated neurodegenerative disease stage with levels of sTREM2; increased levels of CSF sTREM2 have been reported to be a biomarker of Alzheimer's disease severity [31, 32]. Separately, reductions in sTREM2 in the CSF have been used as a biomarker of binding and activation by TREM2 agonist antibodies [33]. Therefore, TREM2 receptor engagement

was confirmed in our microglial assay via measurement of reduced levels of soluble TREM2 released into the media. Consistent with TREM2 target engagement, treatment of microglia with iluzanebart for 24 h led to a dose-dependent decrease in sTREM2 levels detectable in the cell media (Fig. 2C) with an average IC50 of 1.14 nM, similar to its EC50 for phosphorylation of SYK and DAP12.

Iluzanebart increases surface CSF1R levels in healthy microglia

Like TREM2, CSF1R undergoes proteolytic cleavage to generate a soluble fragment. However, unlike TREM2, decreased shedding of soluble CSF1R (sCSF1R) is associated with both disease pathology and homeostasis [34]. Both TREM2 and CSF1R receptors are regulated at the cell surface by an ADAM protease, ADAM17, resulting in cleavage of each receptor and the release of its ectodomain into the surrounding environment to generate a soluble fragment. Additionally, binding of ligands to their respective receptor can result in receptor internalization and an equivalent reduction in soluble receptor levels, as was observed with soluble TREM2. As such, increases in levels of soluble CSF1R in the media can function as a surrogate measurement for the abundance of the receptor at the cell surface.

iMGL treated for 24 h with iluzanebart resulted in a dose-dependent increase in soluble CSF1R levels (Fig. 3A), with an average EC50 of 0.52 nM, when compared to treatment with IgG control, providing a functional readout of iluzanebart in vitro efficacy. We further hypothesized that increases in sCSF1R in the media could be explained by increases in the number of CSF1 receptors at the cell surface. Indeed, this was found to be the case as iluzanebart treatment resulted in increased levels of CSF1R at the cell surface of microglia, as measured by flow cytometry (Fig. 3B and C). When this increase in CSF1R positive microglia was quantified (Fig. 3D), iMGL treated with iluzanebart had a significant, 44.5% increase in surface CSF1R as compared to control IgG. Conversely, microglia that did not express TREM2, (TREM2 -/-) showed no increase in CSF1R levels upon iluzanebart

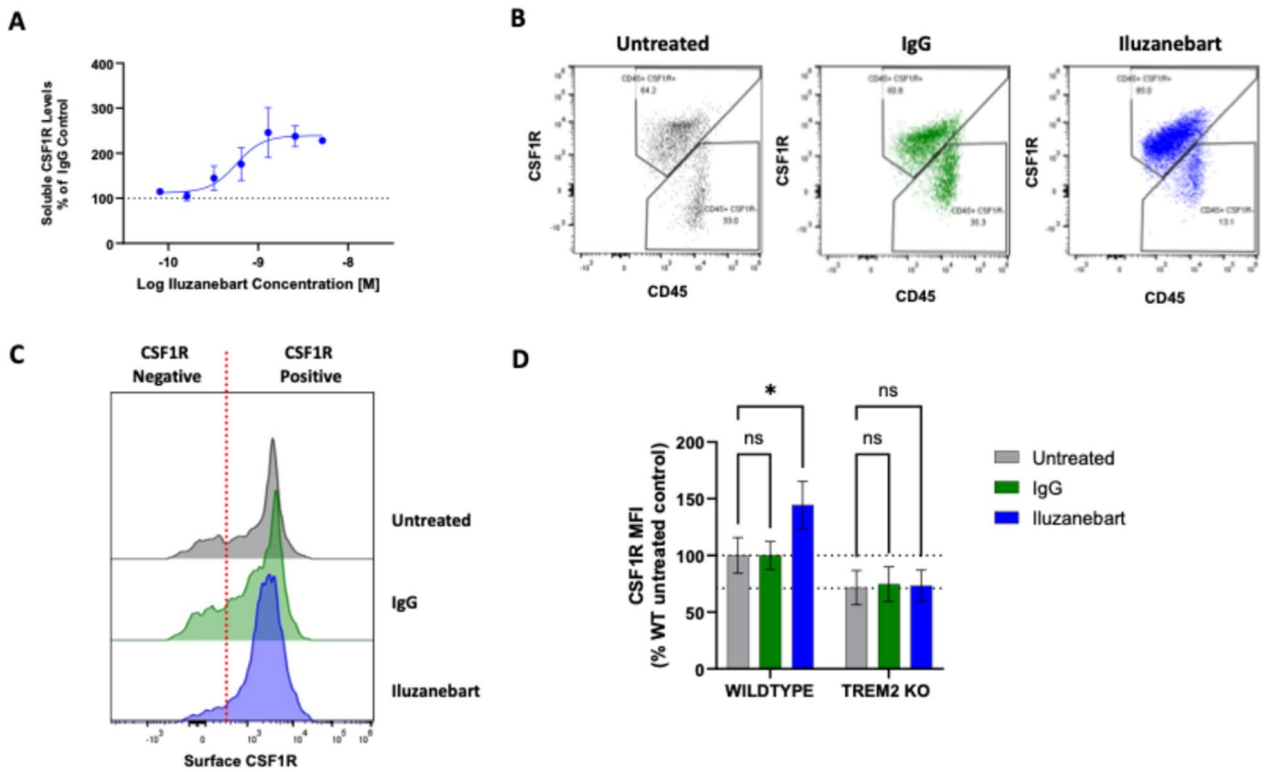

Fig. 3 Iluzanebart increases surface levels of CSF1R. **A iPSC Derived Human Microglia (iMGL).** Treatment of iMGLs with iluzanebart increased levels of soluble CSF1R levels after 24 h, compared to IgG control which had no effect (n = 3 independent experiments). **B** Representative image of population analysis of iMGL post treatment with iluzanebart show increases the population of CSF1R + CD45 + iMGL compared to IgG or untreated control after 24 h. **C** Representative histogram of iMGL shows an increase of surface CSF1R iMGL with iluzanebart. **D** Quantification of mean fluorescence intensity (MFI) demonstrates a TREM2-dependent increase in surface levels of CSF1R by iluzanebart. N = 7 independent experiments for wildtype, n = 5 independent experiments for TREM2 knockout iMGL. Significance was determined by 2-way ANOVA with Sidak's multiple comparison's test. * < 0.05

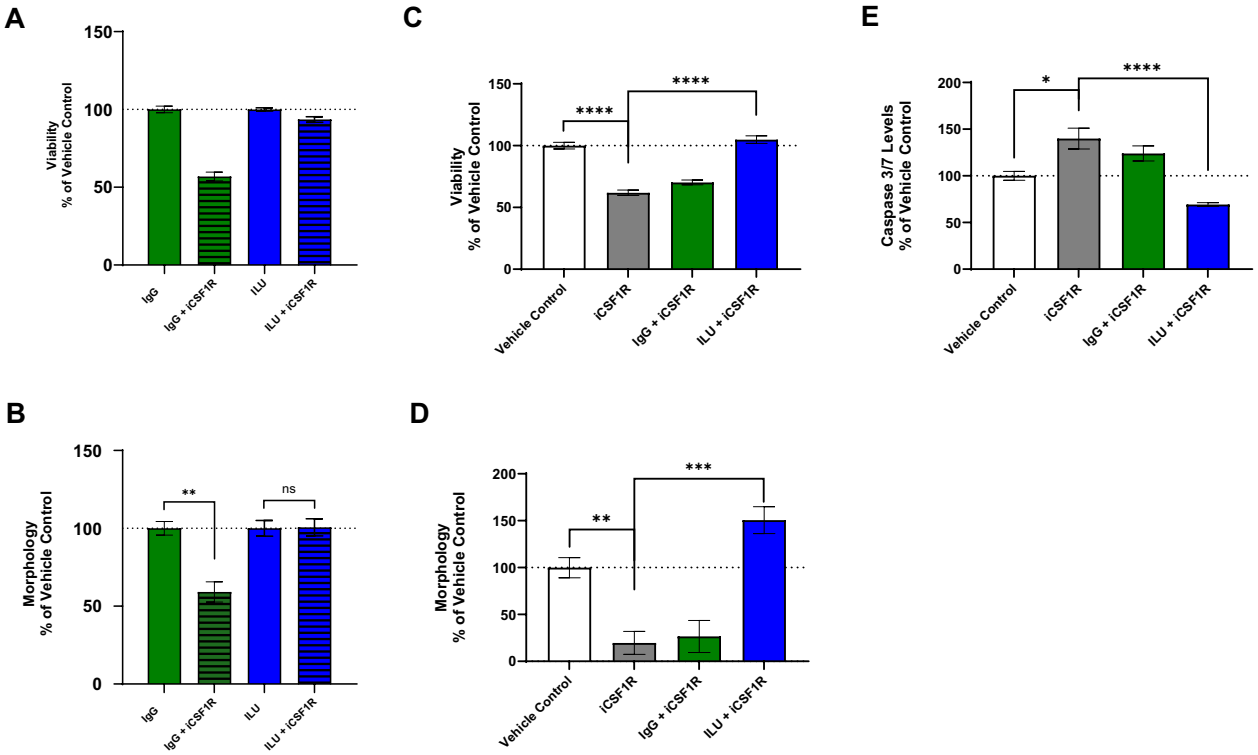

Fig. 4 Iluzanebart (ILU) rescues the effects of CSF1R inhibition in human MDM and iPSC microglia. **A-B Human Monocyte Derived Macrophages (hMDM).** Iluzanebart counteracts the effects of pharmacological CSF1R inhibition on confluence **(A)** and morphology **(B)** of MDMs in vitro (n = 3 independent experiments). Treatment of hMDM cells with PLX5622 (iCSF1R) led to a reduction in cell confluence and morphology (striped bars). Treatment with **i**luzanebart (10 µg/ml; blue bar) restored cellular confluence and ramified morphology, whereas treatment with IgG at the same concentration (green bars) had no effect. **C-E iPSC Derived Human Microglia (iMGL). C** Treatment with PLX5622 (iCSF1R) decreased iPSC microglia cell viability, as measured by CellTiterGlo (grey bar). Treatment with iluzanebart (75 µg/ml; blue bar) led to a significant restoration of viability, whereas treatment with IgG control at the same concentration (green bar) had no effect (n = 4 independent experiments). **D iMGL.** Treatment with PLX5622 (iCSF1R) altered iMGL morphology (grey bar). Treatment with **i**luzanebart (75 µg/ml) restored cellular confluence and ramified morphology (blue bar), whereas treatment with IgG control had no effect (n = 4 independent experiments). **E iMGL.** Treatment with PLX5622 (iCSF1R) (n = 4 independent experiments) increased numbers of caspase 3/7 positive cells in iPSC microglia cultures (grey bar). Treatment with iluzanebart (75 µg/ml) led to a significant reduction in caspase 3/7 + cells (blue bar), whereas treatment with IgG control had no effect (green bar). Significance was determined by one-way ANOVA with Tukey's multiple comparison's test. * < 0.05, ** < 0.05, *** < 0.0005, **** < 0.0001

stimulation, demonstrating that the observed increase in CSF1R levels is entirely dependent on TREM2 activation. Together, these data confirm that iluzanebart directly increases levels of surface CSF1R, as confirmed by multiple assay methodologies.

Iluzanebart rescues the effects of inhibition of CSF1R signaling in human myeloid cells

To investigate the potential of iluzanebart to compensate for the attenuation of CSFR1 signaling that occurs in CSF1R-ALSP, hMDM cells were treated with an IC_{50} concentration of PLX5622, a highly specific, small molecule inhibitor of CSF1R kinase activity that functionally results in the loss of receptor signaling through inhibition of autophosphorylation [33]. The effect of iluzanebart treatment on cell viability and morphology, which are observed to be altered in CSF1R-ALSP individuals, was assessed following treatment with PLX5622.

Treatment of hMDMs with 1 µM PLX5622 (the experimentally determined IC_{50} concentration) in the presence of 10 µg/ml IgG resulted in a significant decrease in the percentage of viable cells in the culture (Fig. 4A, green bars). However, in the presence of 10 µg/ml iluzanebart, no significant decrease in viability was detected following PLX5622 treatment (4A, blue bars). Similarly, iluzanebart protected microglia from changes in confluence and cellular morphology in cultures treated with PLX5622, whereas the IgG control did not (Fig. 4B). This effect was likewise seen in iMGL cultures that were treated

with PLX5622. Cell viability (Fig. 4C) and morphology (Fig. 4D) were both reduced by PLX5622 treatment and rescued by treatment with iluzanebart, but not by the matched IgG control. This improvement in cell viability was demonstrated to be acting via inhibition of apoptosis, as a statistically significant decrease in PLX5622-induced caspase 3/7 staining in iMGL cultures was observed following treatment with iluzanebart (Fig. 4E). Thus, iluzanebart was able to reverse the effects of CSF1R functional inhibition on all CSF1R-ALSP-relevant phenotypes measured in disease relevant primary cells.

Iluzanebart rescues the effects of complete loss of CSF1R signaling in human myeloid cells

While the CSF1 receptor contains multiple intracellular domains that are responsible for transmission of the downstream signaling cascade, the extracellular domain consists of five IgG like domains, and is responsible for binding of its ligands, CSF1 and IL34 [34]. In the absence of a ligand, CSF1R can still dimerize, but remains in an auto-inhibited state, preventing autophosphorylation and subsequent downstream signaling. Due to this autoinhibition, withdrawal of CSF1 from culture media has been demonstrated to induce loss of CSF1R signaling, resulting in loss of viability in human myeloid cells. Conversely, agonism of TREM2 under low CSF1 conditions has been shown to rescue hMDM from apoptosis and promote survival [11, 24, 25].

To investigate whether the protective effect of iluzanebart is seen in the context of complete ligand withdrawal to reduce CSF1R signaling, hMDM and iMGL cultures were each placed in withdrawal media lacking CSF1. In hMDM cultures, CSF1 withdrawal resulted in a significant increase in apoptosis, as measured by caspase 3/7 staining (Fig. 5A, grey bar), and resulted in a significant change in morphology as measured by a decrease in cell confluence (Fig. 5B, grey bar, 5F). While treatment with its IgG control yielded no rescue of these effects (green bars), treatment of hMDM with iluzanebart resulted in a statistically significant reversal of both cell viability and of morphological changes (blue bars). The same effect was observed when cultures of iMGL were placed in CSF1 withdrawal media and subsequently treated with either IgG or iluzanebart; cell viability (Fig. 5C), morphology (Fig. 5D and 5G), and levels of caspase activation (Fig. 5E) were all restored by iluzanebart treatment. Thus, iluzanebart was able to rescue the effects of CSF1R inhibition in two independent models of CSF1R hypofunction, in two different human myeloid cell types.

Iluzanebart rescues the effects of a CSF1R-ALSP relevant CSF1R mutation in CRISPR-edited microglia

The I794T mutation in the CSF1 receptor is one of many observed mutations in the kinase domain that renders CSF1R functionally inactive. It is also the most frequently observed mutation reported in an ongoing natural history study of CSF1R-ALSP [35]. This mutation was introduced into an apparently healthy normal iPSC line, ASE-9211 using CRISPR-Cas9. The resulting progenitor cells ($I794T^{+/-}$) were differentiated to monocytes, harvested, plated onto IgG- or iluzanebart-coated cell culture plates, and incubated for seven days to complete the differentiation process to microglia, utilizing a CSF2/IL34 driven differentiation protocol [36]. At this point, viability, soluble, total, and phospho-CSF1R (pCSF1R) levels were each assessed. In $I794T^{+/-}$ iMGL, viability was significantly increased in iluzanebart-treated cultures compared to IgG-treated controls (Fig. 6A). Additionally, as observed in CSF1R-ALSP patients, levels of both soluble CSF1R, total CSF1R, and phospho-CSF1R were significantly lower in $I794T^{+/-}$ microglia as compared to wildtype microglia; 38%, 23%, and 34% respectively. While iluzanebart treatment did not affect levels of total CSF1R levels in either cell line (Fig. 6B), ILU treatment increased levels of soluble CSF1R in cultures of both $I794T^{+/-}$ and wildtype cells (Fig. 6C). Additionally, while iluzanebart treatment resulted in a modest increase in "activated" CSF1R as measured by phospho-CSF1R levels in wildtype microglia, phospho-CSF1R levels were significantly increased in $I794T^{+/-}$ cells, with levels of phospho-CSF1R restored to that of healthy wildtype cells. This increase translates to a significant increase of 2.26× in the ratio of phosphorylated to total CSF1R levels in $I794T^{+/-}$ cells (Fig. 6D, E). Interestingly, no effect on total CSF1R levels was observed, suggesting that this effect is limited to alterations in levels of CSF1R at the cell surface, and is not due to changes in transcription of CSF1R or in cell number. Together, these data suggest that iluzanebart has the potential to restore levels of CSF1R signaling in CSF1R-ALSP patient microglia to levels observed in healthy individuals.

Iluzanebart concentrations in mouse plasma and brain

Next, as iluzanebart is specific for human TREM2, the effects of iluzanebart treatment were assessed in mice that are engineered to express human TREM2 but lack expression of murine TREM2 (hTREM2-CV). These mice have been extensively profiled by others, and microglia from hTREM2 expressing mice have been shown to fully recapitulate the function and behavior of endogenous microglia [20, 25, 37, 38]. First, to validate that iluzanebart is human specific, we have demonstrated that iluzanebart shows no ability to bind and activate rodent

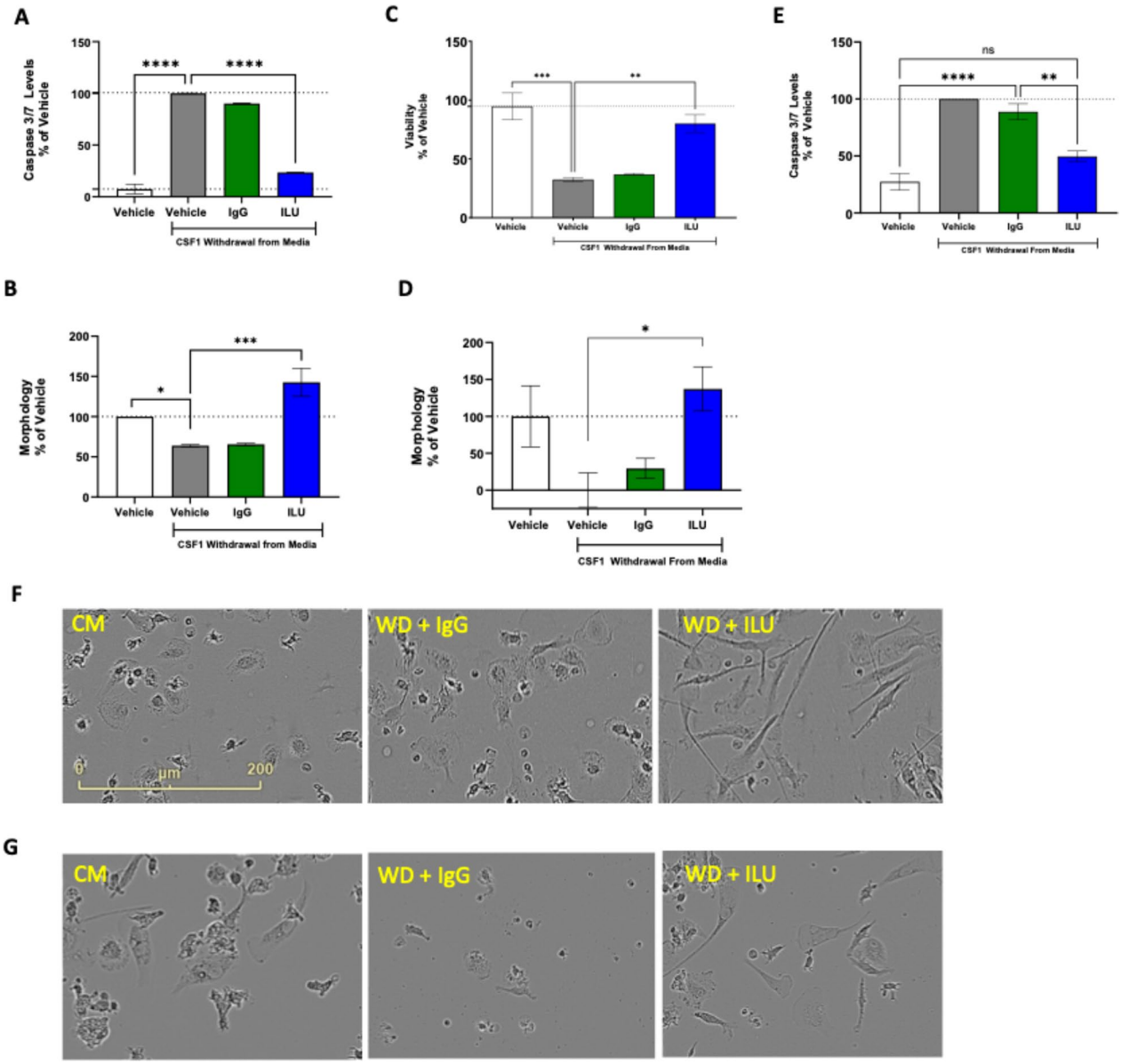

Fig. 5 Iluzanebart (ILU) increases survival and restores morphology of human MDMs and iPSC microglia following CSF1 withdrawal in vitro. **A**-**B Human Monocyte Derived Macrophages (hMDM)**. Iluzanebart counteracts the effects of CSF1 withdrawal-induced apoptosis and morphology in hMDM cultures from 2 independent monocyte donors **(A) hMDM.** Withdrawal of CSF1 from the culture media increased caspase 3/7 + cells in human MDM cultures (grey bar). Treatment of cells with iluzanebart (10 µg/ml, blue bar) led to a significant reduction in caspase 3/7 + cells, whereas treatment with IgG (green bar) did not. **B hMDM**. Withdrawal of CSF1 reduced confluence of cells in human MDM cultures (grey bar). Treatment of cells with iluzanebart (10 µg/ml, blue bar) led to a significant increase in confluence, whereas treatment with IgG (green bar) did not. **C-E iPSC Derived Human Microglia (iMGL). C** Withdrawal of CSF1 decreased iMGL cell viability (n = 3 independent experiments), as measured by CellTiter Glo (grey bar). Treatment with iluzanebart (75 µg/ml, blue bar) led to a significant restoration of ATP levels, whereas treatment with IgG control (green bars) did not. **D iMGL.** Withdrawal of CSF1 from the culture media decreased morphological eccentricity (n = 5 independent experiments) of human iPSC-derived microglia in vitro (grey bar). Treatment with iluzanebart (75 µg/ml, blue bar) restored cellular morphology to a more ramified state, whereas treatment with IgG control (green bar) did not. **E iMGL.** Withdrawal of CSF1 increased caspase 3/7 + cells (n = 5 independent experiments) in iPSC microglia cultures (grey bar). Treatment with iluzanebart (75 µg/ml, blue bar) led to a significant reduction in caspase 3/7 + cells, whereas treatment with IgG control (green bar) did not. **F hMDM.** Representative images of cells in complete media (CM), cells in withdrawal media treated with IgG control (WD + IgG), and cells in withdrawal media exposed to iluzanebart (WD + ILU). **G iMGL.** Representative images of cells in complete media (CM), cells in withdrawal media treated with IgG control (WD + IgG), and cells in withdrawal media exposed to iluzanebart (WD + ILU). Significance was determined by one-way ANOVA with Tukey's multiple comparison's test, * < 0.05, ** < 0.05, *** < 0.0005, **** < 0.0001

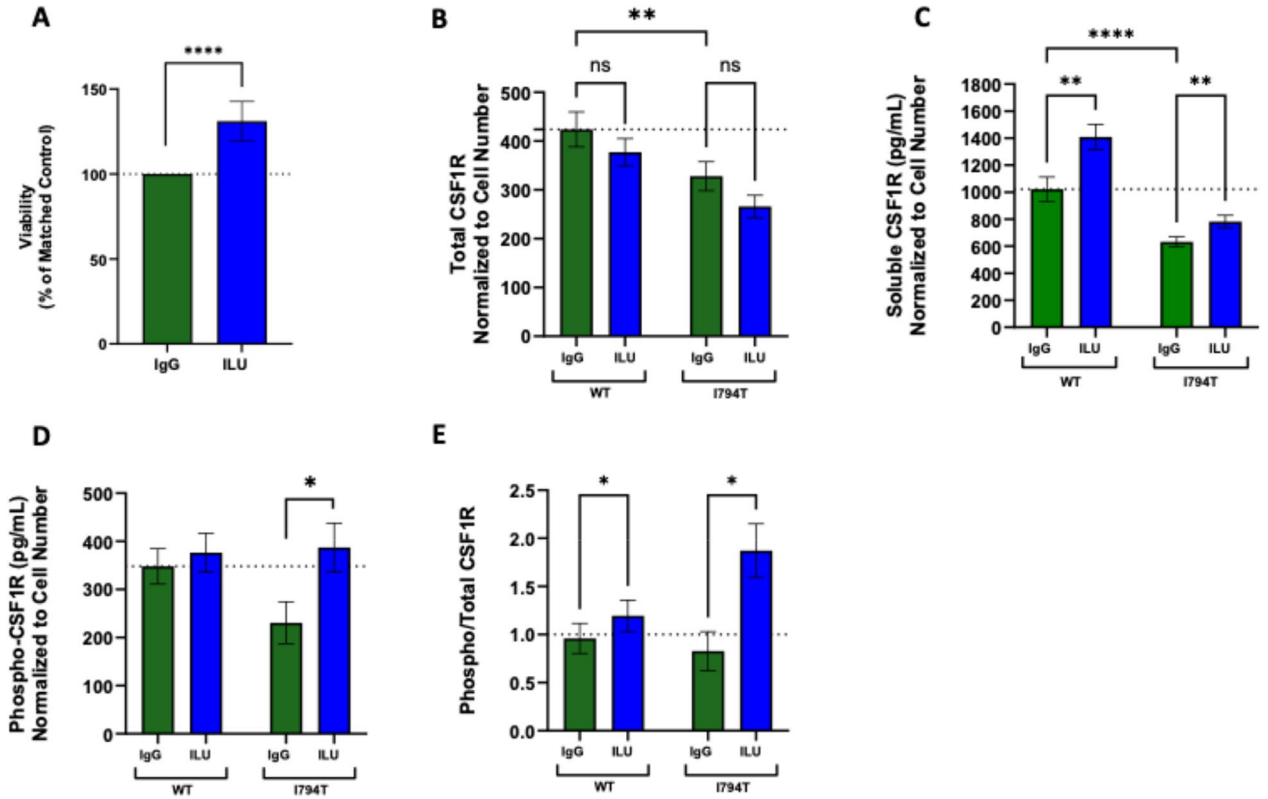

Fig. 6 Iluzanebart (ILU) increases viability and restores CSF1R activity in CRISPR-generated I794T$^{+/-}$ mutant iPSC microglia. iPSC microglia generated to heterozygously express the I794T CSF1R mutation were harvested, plated onto IgG- or iluzanebart-coated surfaces (ILU), and incubated for 7 days before analysis. Cultures were assessed for viability by CellTiterGlo, soluble CSF1R in the media by ELISA, or for phospho-CSF1R levels in the cells by ELISA. **A** In I794T$^{+/-}$ microglia, viability was significantly increased in iluzanebart-treated cultures compared to IgG-treated controls (n = 9 independent experiments). **B** While iluzanebart treatment did not significantly affect levels of total CSF1R in either WT or I794T$^{+/-}$ cells, total CSF1R levels were 23% lower in I794T$^{+/-}$ cells compared to WT cells (n = 9 independent experiments). **C** While soluble CSF1R levels were 38% lower in I794T$^{+/-}$ cell culture media compared to WT, iluzanebart treatment significantly increased levels of soluble CSF1Rin both cultures (n = 9 independent experiments). **D** While iluzanebart treatment had no impact on phosphorylation of CSF1R in WT cells, phospho-CSF1R levels were 34% lower in I794T$^{+/-}$ cells compared to WT, and iluzanebart treatment restored pCSF1R levels to normal WT levels. (n = 9 independent experiments). **E** While iluzanebart treatment slightly increased the ratio of activated CSF1R in WT cells, activated CSF1R levels were increased 2.26 × in I794T$^{+/-}$ cell cultures (n = 9 independent experiments). All data were normalized to cell number as determined using Incucyte cell number determination. Significance was determined by two-way ANOVA with Tukey's multiple comparison's test, * < 0.05, ** < 0.005, **** < 0.0001

TREM2, as no induction of SYK phosphorylation was observed in HEK293T cells engineered to express rodent TREM2 and DAP12 receptors (Supplementary Fig. 3A and B). Treatment with iluzanebart failed to induce SYK phosphorylation below concentrations of 1000 nM, while a positive control antibody that cross reacts with both mouse and human TREM2 did result in SYK phosphorylation. Therefore, the observed activity in vivo is limited exclusively to agonism of human TREM2.

Iluzanebart concentrations were determined in plasma samples from equal numbers of adult male and female mice at 1, 2, 4, 8 and 24 h post dose, and in brain tissues 24 h post dose, following single intraperitoneal (IP) administration of iluzanebart at 1, 3, 10, 30, 100, and 200 mg/kg in healthy hTREM2-CV mice. All mice survived treatment, and no treatment related signs of toxicity were observed. Plasma concentration–time profiles are shown in Supplemental Fig. 4, with maximal concentrations were observed between 2 and 8 h post dose, and plasma exposure of iluzanebart increased in an apparently proportional manner from 1 to 30 mg/kg (Fig. 7). At 24 h post dose, the measured total brain concentrations were approximately 0.1% of plasma concentrations and increased dose proportionally from 1 to 200 mg/kg. At the 10 mg/kg dose, brain concentrations were within range of the in vitro iMGL pSYK EC_{50} value, as well as the sCSF1R and sTREM2 EC_{50} values.

A

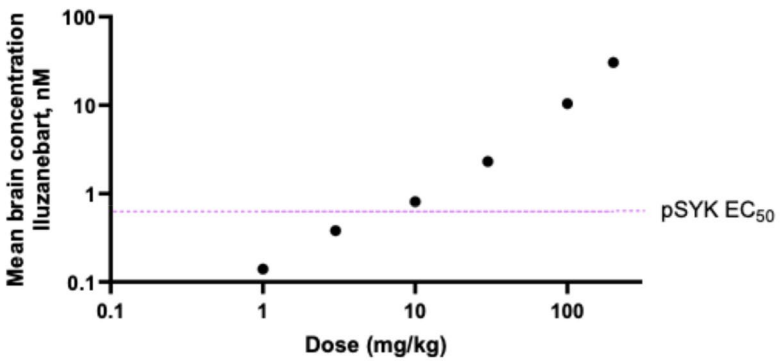

B

Dose	Brain concentration		Brain/Plasma Ratio	Brain Concentration/EC50		
mg/kg	ng/mL	nM	%	pSYK	sCSF1R	sTREM2
1	20.3 ± 8.67	0.1	0.15 ± 0.05	0.2	0.2	0.1
3	57.2 ± 25.5	0.4	0.13 ± 0.07	0.6	0.8	0.4
10	121 ± 39.2	0.8	0.08 ± 0.02	1.3	1.5	0.7
30	346 ± 66.0	2.3	0.08 ± 0.04	3.7	4.4	2.0
100	1560 ± 499	10.4	NA	16.5	20.0	9.1
200	4580 ± 1580	30.5	NA	48.4	58.7	26.8

Fig. 7 Pharmacokinetic analysis of iluzanebart in hTREM2-CV mice. Terminal iluzanebart brain concentrations and corresponding fold exposures over iluzanebart in vitro sCSF1R EC_{50} and sTREM2 IC_{50} pharmacologically align with on-target TREM2 agonism. Values are reported as mean ± standard deviation, n = 4–6 mice per group. **A** hTREM2-CV mice were dosed intraperitoneally with a single dose of iluzanebart, and brain and plasma concentrations were measured 24 h later. A minimal dose of 10 mg/kg was shown to achieve brain levels equal to or higher than the pSYK EC50 in iPSC derived microglia. **B** Terminal iluzanebart brain concentrations and corresponding fold exposures over iluzanebart in vitro sCSF1R EC_{50} and sTREM2 IC_{50}. Iluzanebart Plasma concentrations of iluzanebart in the 100 and 200 mg/kg dose groups was above the limit of quantitation and was therefore excluded

Transcriptomic profiling and pathway analysis in iluzanebart-treated mice

Hippocampal tissues were collected from the same hTREM2-CV transgenic mice utilized in the same pharmacokinetic study following single IP administration of iluzanebart at 10, 30, 100, or 200 mg/kg or control IgG at 100 mg/kg. RNA isolated from the hippocampus was analyzed using RNAseq, and differentially expressed genes in the tissues from iluzanebart-treated mice relative to control IgG-treated mice are shown in Fig. 8A and Supplementary File 1. After 200 mpk iluzanebart treatment, 128 genes with adjusted p values of less than 0.05 were determined to be significantly differentially expressed. The 100 mpk dose yielded 97 significant DEGs, but of those genes, a significant amount, 36%, were similarly differentially expressed in the 200 mpk group after iluzanebart treatment. In the 30 mpk and 10 mpk groups, fewer genes were determined to be significantly differentially expressed; with 27 and 16 genes differentially expressed, respectively.

Genes that were significantly upregulated by iluzanebart at 200 mg/kg compared to IgG control included genes involved in chemotaxis and immune activation and regulation (Ccl12, Cxcl10, and Gpr84), proliferation (Fam11a, Mki67, Top2a, Uhrf1), and homeostasis (Dusp1, Fcrls, Itgb2, and Olfml3). While these mice do not exhibit any neurodegenerative disease pathology, some neuroprotective, disease associated microglia (DAM) genes were still detected as upregulated. DAM genes whose expression increased greater than 0.25 log2 fold included Cst7, Ccl3, Ccl6, Cd52, Cd68, Clec7a, Cxcl16, Ctsz, Fgl2, Itgax, SlamF9, and Tyrobp [39]. Other DAM genes that were significantly upregulated, but less than 0.25 log2 fold included Axl, B2m, Cd9, Gusb, H2-d1, Hif1a, and Lpl. The most significantly affected pathway was determined to be proliferation related pathways, with 14% of total DEGs at 200 mpk relating to proliferation and having a log2 fold change of > 0.3.

Confirming previous data, no change in expression of CSF1R was observed at 24 h, suggesting that the increase in surface levels of CSF1R on microglia is not due to increased gene expression. All differentially expressed genes (adjusted p value ≤ 0.05) as compared to the IgG control for the 200 mg/kg group were analyzed using STRING (Fig. 8B). STRING analysis showed that differentially expressed genes self-assembled into "nodes"

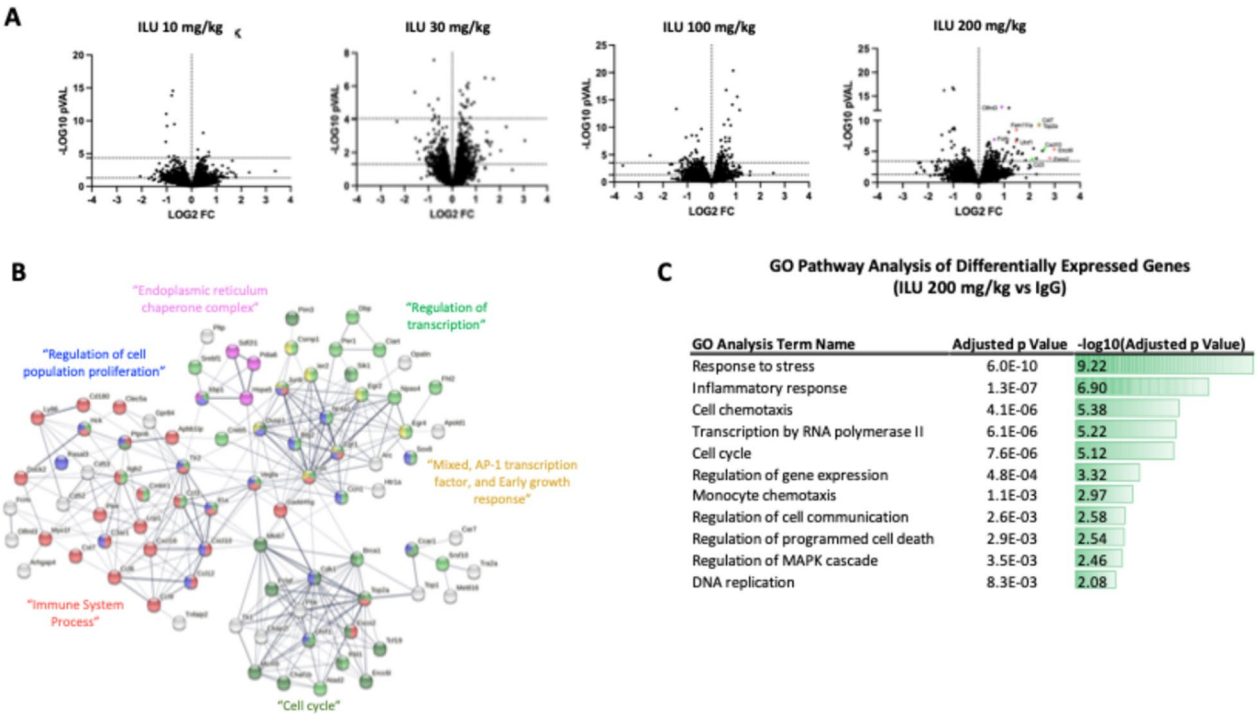

GO Analysis Term Name	Adjusted p Value	-log10(Adjusted p Value)
Response to stress	6.0E-10	9.22
Inflammatory response	1.3E-07	6.90
Cell chemotaxis	4.1E-06	5.38
Transcription by RNA polymerase II	6.1E-06	5.22
Cell cycle	7.6E-06	5.12
Regulation of gene expression	4.8E-04	3.32
Monocyte chemotaxis	1.1E-03	2.97
Regulation of cell communication	2.6E-03	2.58
Regulation of programmed cell death	2.9E-03	2.54
Regulation of MAPK cascade	3.5E-03	2.46
DNA replication	8.3E-03	2.08

Fig. 8 Bulk RNAseq analysis of iluzanebart-treated (ILU) mouse hippocampal tissue reveals differentially expressed genes. **A** Volcano plots of differentially expressed genes in hippocampus harvested from iluzanebart-treated (10, 30, 100, and 200 mg/kg) hTREM2 knock-in mice vs. IgG control-treated, n = 4–6 mice per group. **B** STRING analysis of genes of interest revealed gene clusters related to proliferation/ DNA replication, innate immune response, endoplasmic reticulum and protein folding, and AP-1/ transcription activation. **C** Gene ontology terms found to be associated with the differentially expressed genes ($p < 0.05$) are listed, ranked by adjusted p-value

around different TREM2 related processes. These processes were representative of both TREM2 and CSF1R related pathways, including immune system process, regulation of proliferation, regulation of transcription, AP-1 transcription factor and early growth response, among others.

Finally, the gene ontology (GO) terms describing the top differentially expressed pathways affected by changes in gene expression are listed in Fig. 8C. Pathways that were significantly affected by iluzanebart treatment also included TREM2 and CSF1R relevant pathways; response to stress, inflammatory response, chemotaxis, transcription, and cell cycle, among others. Overall, iluzanebart treatment of healthy hTREM2-CV mice resulted in changes in gene expression indicative of TREM2 activation, but also changes in gene expression that overlap with CSF1R-related pathways.

Iluzanebart induces TREM2 specific chemokine increases in vivo

Levels of specific proteins, guided by the genes that were highlighted in the RNAseq analysis, were determined in cortical tissue lysates isolated from the same iluzanebart or IgG-treated hTREM2-CV mice using MesoScale Discovery assays. Of note, IP10 (Cxcl10) was increased 2.59 log2 fold (adjusted p value = 0.0018) in the 200 mpk group compared to IgG control, while Ccl3 (Mip1α) was increased 2.11 log2 fold (adjusted p value = 0.029). Iluzanebart treatment significantly increased protein expression of IP10 and MCP1 at 100 and 200 mg/kg, and MIP1α at doses of ≥ 10 mg/kg in hTREM2-CV mice (Fig. 9A-C). In contrast, iluzanebart treatment (200 mg/kg) had no effect on the protein levels of IP10, MCP1, and MIP1α in the cortical tissues collected from a separate cohort of mice lacking human TREM2 (Fig. 9D), demonstrating that this effect is entirely dependent on TREM2. Additionally, levels of IL15, a non-TREM2 dependent cytokine, were not affected by iluzanebart treatment, and were similar between cortices from hTREM2-CV and hTREM2 -/- mice, demonstrating again that cytokine modulation is specific and TREM2 dependent. Therefore, iluzanebart treatment resulted in gene expression changes in mice that were TREM2 relevant, and these gene expression changes translated to changes in protein levels.

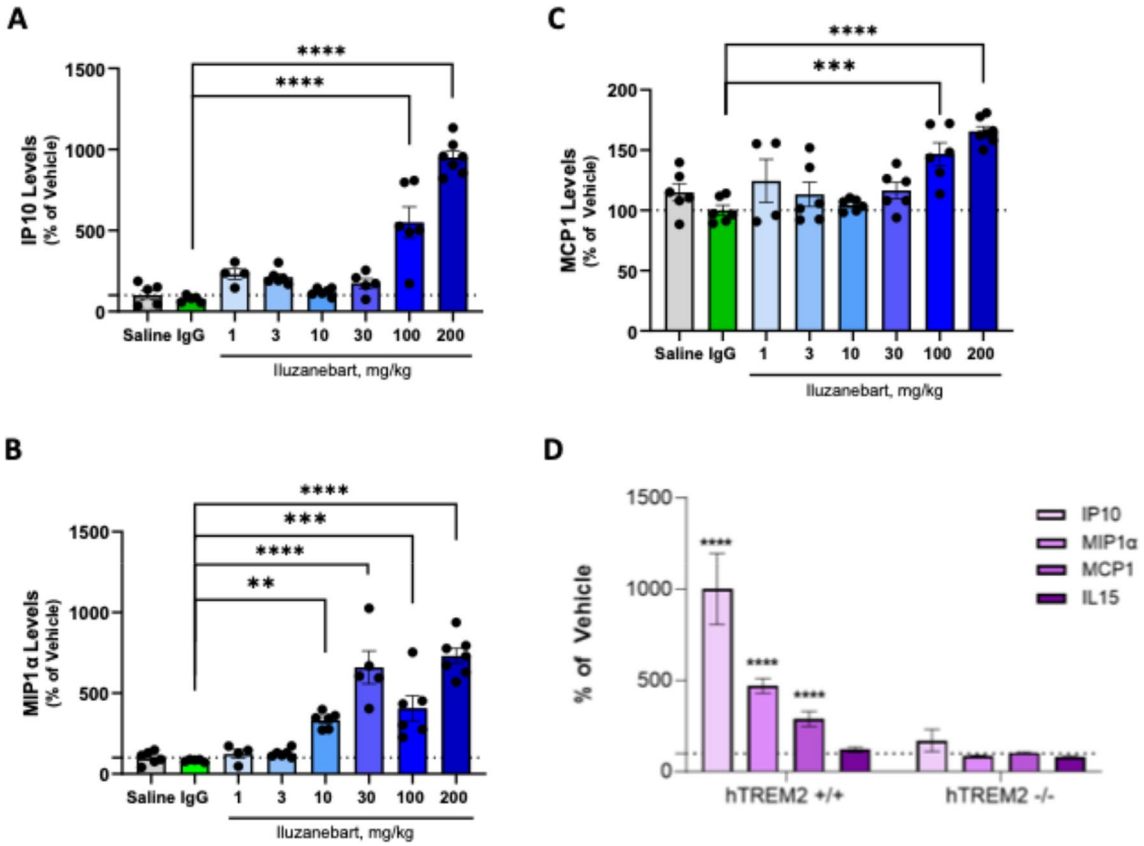

Fig. 9 MSD analysis of iluzanebart-treated mouse cortical tissue reveals dose-dependent, TREM2-dependent changes in cytokine levels. **A-C** hTREM2-CV mice (n = 4–6 mice per group) were treated with iluzanebart (IP; 1, 3, 10, 30, 100, or 200 mg/kg), IgG (100 mg/kg), or saline. Cortical tissue was harvested 24 h after treatment. Levels of the cytokine IP10 **(A)**, MIP1α **(B),** and MCP1 **(C)** showed a dose–response effect in response to iluzanebart treatment, whereas IgG-treated had no change in levels in any of these factors compared to saline-treated controls. **D** Cytokine levels measured by MSD in cortical tissue from hTREM2$^{+/+}$ mice or hTREM2.$^{-/-}$ mice, perfused and collected 24 h after intraperitoneal dose of 200 mg/kg iluzanebart. Three chemokines expected to respond to TREM2 agonism demonstrated a significant increase relative to vehicle after 24 h, while no significant increase in these chemokines was observed in mice lacking TREM2. IL15, a cytokine not expected to respond to TREM2 agonism, was included as a negative control. Data shown is reported as % of vehicle control. Significance was determined by one-way ANOVA with Dunnett's multiple comparison's test, * < 0.05, ** < 0.05, *** < 0.0005, **** < 0.0001

Iluzanebart induces proliferation of microglia in vivo

Finally, equal numbers of adult male and female hTREM2-CV mice were dosed intraperitoneally with either iluzanebart at 200 mpk, IgG at 200 mpk, or an equal volume of sterile saline solution, and 48 h later, whole brain tissue was harvested for flow cytometric analysis. Following tissue dissociation and myelin removal, cells were sorted by CD45 and CD68 expression to identify microglial populations, and then analyzed for human IgG for target engagement, Ki67 as a marker of proliferation, and CSF1R. Samples without detectable human IgG, and therefore without measurable iluzanebart or IgG, were excluded from the analysis (Supplemental Fig. 5). As seen in Fig. 10, iluzanebart treatment significantly increased the number of Ki67 positive microglia in vivo by 192.3%. While the IgG control resulted in a smaller increase in Ki67 positive microglia, this increase (69.7%) was not statistically significant (Fig. 10A). This confirms that the transcriptional signature for proliferation observed in vitro translates in vivo to proliferation of microglia. Additionally, CSF1R levels were analyzed, and a representative histogram is seen in Fig. 10B. Strikingly, a significant increase in microglia with high CSF1R levels is observed (Blue circle). When quantified (Fig. 10C), this translates to a significant, 60.1% increase in MFI in the iluzanebart treated group, whereas no change was observed in the IgG control treated group. These data demonstrate that not only does the transcriptional reprogramming observed in iluzanebart treated mice translate to proliferation of microglia, but this also translates to a population of microglia with increased CSF1R levels; both being critical to rescue loss of microglia and hypofunction of CSF1R signaling seen in CSF1R-ALSP individuals.

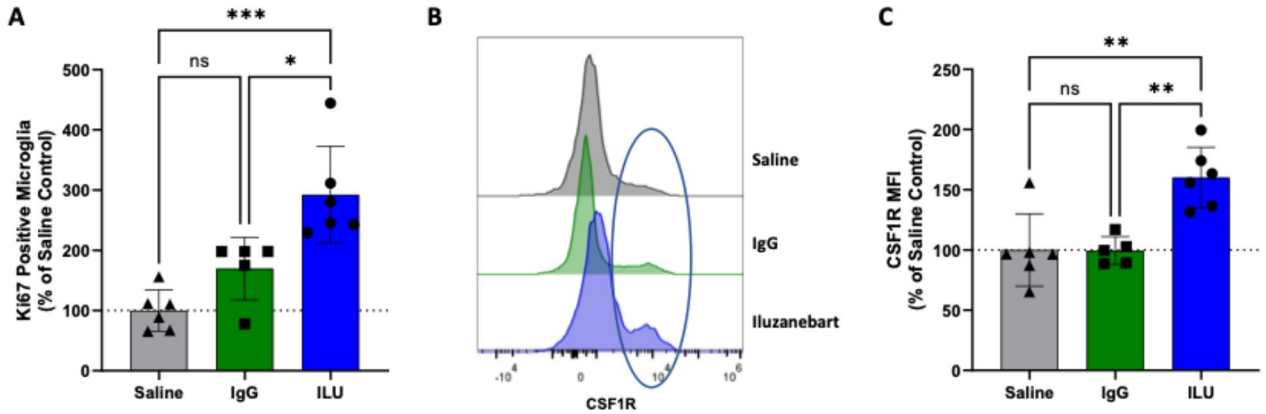

Fig. 10 Iluzanebart induces proliferation and increases CSF1R levels in microglia in vivo. hTREM2-CV mice were dosed intraperitoneally with a single, 200 mg/kg dose of either iluzanebart or IgG control, or an equal volume of saline. Brain tissue was harvested 48 h after dosing, enzymatically digested, and cells stained with Ki67, CSF1R, CD45, CD68, and human IgG. Only mice with detectable human IgG present in the sample were analyzed. **A** Analysis of microglia post iluzanebart dosing show a significant increase in the number of Ki67 positive microglia compared to IgG or saline control. **B** Representative histogram shows an increase in population of cells with high CSF1R expression (blue circle) in microglia with Iluzanebart treatment. **C** Quantification of mean fluorescence intensity (MFI) demonstrates an increase in cells with high CSF1R by Iluzanebart treatment. N = 5–6 mice per group. Data shown is reported as % of saline control. Significance was determined by one-way ANOVA with Tukey's multiple comparison's test, * < 0.05, ** < 0.005, *** < 0.0005

Discussion

Herein we describe the preclinical pharmacological and functional profile of iluzanebart, a human TREM2 (hTREM2) agonist antibody, as a microglial targeting, potentially disease modifying immunotherapy currently in clinical development for CSF1R-ALSP. The pharmacodynamic effects of iluzanebart were assessed in two human primary cell types, hMDMs and iMGLs, and in two models of CSF1R deficiency: rescue of PLX5622 induced CSF1R hypofunction, and rescue of the more complete elimination of CSF1R signaling through ligand withdrawal. These two separate approaches to modeling CSF1R deficiency facilitate the assessment of various aspects of CSF1R-ALSP functional pathology. PLX5622 treatment models the CSF1R haploinsufficiency observed in CSF1R-ALSP patients by facilitating titration of inhibition to a 50% reduction in CSF1 receptor activity. In this model, iluzanebart not only increased cellular viability but also reduced levels of apoptosis (as measured by caspase 3/7 activity) and returned the morphology of the cells to a more ramified (as measure by increased eccentricity) and less "activated" state. The observed rescue of morphology is a critical observation: in post-mortem brain tissue from CSF1R-ALSP patients, reduced numbers of microglia are observed, while the remaining microglia exhibit a less ramified morphology. Withdrawal of CSF1 from culture media, resulting in near complete loss of function of CSF1R, models near complete loss of function of CSF1 receptors. In this highly inhibited state, iluzanebart again rescued cell viability, reduced levels of caspase-mediated apoptosis, and returned cell morphology to that of a homeostatic, ramified state. This suggests that iluzanebart can rescue both microglia cell numbers and the abnormal activation state of the cell, both of which are observed in the CNS of CSF1R-ALSP individuals.

CRISPR-edited I794T$^{+/-}$ iPSC-derived microglia were used to model the most common CSF1R-ALSP mutation observed in patients. In these microglia, iluzanebart not only increased cell viability, but also increased levels of CSF1R activation (via phospho-CSF1R) with no effect on total levels of CSF1R. The mechanism of iluzanebart-mediated increases in CSF1R activation requires further investigation. Regardless, the inclusion of iMGL differentiated from CRISPR-generated iPSC microglia containing a mutation found in CSF1R-ALSP individuals supports the clinical relevance of these findings; consistent results across all models of CSF1R deficiency-related disease suggest that agonism of TREM2 with iluzanebart improves overall microglia survival and function, independent of the method of CSF1R signaling attenuation. As the heterozygous nature of the mutation in this model system can recapitulate the haploinsufficiency that individuals with CSF1R mutations experience in CSF1R-ALSP, these findings may be highly clinically relevant.

In vitro models of CSF1R-ALSP were utilized in these experiments due to the lack of translationally relevant rodent transgenic models that recapitulate CSF1R loss of function phenotypes observed in individuals with CSF1R-ALSP. A handful of prior studies have sought to model CSF1R-ALSP via heterozygous deletion of CSF1R, however these mice exhibit either increased microglial

density or no changes in microglia numbers at all, thus failing to recapitulate the underlying cause of human CSF1R-ALSP: microglial hypofunction and apoptosis [40, 41]. Likewise, heterozygous deletion of CSF1R in rats did not lead to any detectable phenotypes in the CNS [42]. More recently, some of the cardinal features of CSF1R-ALSP have been reported in aged, homozygous ΔFIRE mice, a mouse model which lacks CSF1R expression via loss of the fms-intronic regulatory element. Paradoxically, in this model, some CSF1R-ALSP features do occur, but it is via slowly progressing neuropathology [43], unlike the rapid progression observed in CSF1R-ALSP individuals. While some hallmarks of CSF1R-ALSP such as astrogliosis, calcification, and axonal spheroids align with the clinical pathology of CSF1R-ALSP, the loss of microglia in this model is total and complete, and therefore not fully representative of CSF1R-ALSP. While the ΔFIRE model is clearly a useful model, the key limitation of the ΔFIRE mouse model is the inability to support the assessment of therapeutic approaches aimed at targeting the residual population of microglia that remain in the CSF1R-ALSP brain, which iluzanebart does.

Overall, this lack of translational CSF1R-ALSP mouse models that faithfully recapitulate human CSF1R-ALSP disease pathophysiology led us to focus directly on efficacy studies in human primary myeloid and iPSC derived microglial models, while using hTREM2-CV mice exclusively for pharmacokinetic and pharmacodynamic studies. Given the exquisite specificity of iluzanebart for human TREM2, the well characterized hTREM2-CV expressing mice were necessary for understanding the pharmacokinetic and pharmacodynamic profile of iluzanebart. While results from in vitro studies are somewhat limited in translatability of these results to patients in the clinic, restoration of CSF1R signaling in human iPSC derived microglia carrying a mutation found in CSF1R-ALSP individuals presents an exciting and highly disease relevant result that could directly translate to clinical outcomes.

Following single IP administration of iluzanebart in hTREM2-CV mice, brain exposure of iluzanebart appeared to be similar to the reported brain penetration of antibodies in mice with brain to plasma concentration ratios of ~ 0.1% [44]. Iluzanebart induced gene expression profiles that were both TREM2-relevant and CSF1R-relevant and demonstrated a positive impact on microglia via increased viability and increased CSF1R related signaling and pathways. Increases in genes involved in proliferation, TREM2 activation (e.g., innate immune response), homeostatic genes (suggesting an increase in microglial numbers), and DAM genes (neuroprotective phenotype) suggest a restoration of signaling through DAP12 lost in CSF1R haploinsufficiency by TREM2 activation. Iluzanebart treatment increased protein levels of the three chemokines examined; IP10 (CXCL10), MIP1α (CCL3), and MCP1 (CCL2), at doses ≥ 10 mg/kg. In addition, these effects were determined to be TREM2 specific and dependent, as mice lacking TREM2 (TREM2 -/-) showed no increase in these chemokines upon iluzanebart treatment. These changes were also limited to specific, TREM2 dependent chemokines, as no change in IL15 was observed with iluzanebart treatment. Finally, building on the proliferation signal observed in these pharmacodynamic studies, iluzanebart treatment of hTREM2 mice resulted in a significant increase in proliferating microglia 48 h post dose, as well as an increase in microglia expressing high levels of CSF1R.

Together, these results support the hypothesized iluzanebart molecular mechanism of action, as depicted in Fig. 11. A potent and selective agonist of TREM2 activity, iluzanebart compensates for CSF1R signaling deficiency through the well-described, convergent molecular signaling pathway and shared functional role of TREM2. It is also possible that a direct interaction between CSF1R and TREM2 exists; this hypothesis requires further investigation. However, no transcriptional differences in TREM2 or TREM2-related pathway genes were observed between the wildtype or $I794T^{+/-}$ microglia after 7 days in differentiation culture via TempoSeq (data not shown), but it is possible that basal differences could have been masked by the alternative, CSF2 driven method required for differentiation of CSF1R deficient cells to microglia.

While other TREM2 agonist antibodies have been evaluated in multiple neurogenerative mouse models with mixed results [43], these antibodies were not tested in specific models of CSF1R-ALSP. Although a recent study suggests that complete loss of TREM2 signaling improves myelination in $CSF1R^{+/-}$ mice, a finding that apparently contradicts our conclusion that bolstering TREM2 signaling will improve neuronal health, likely these results could be explained by differences in the mouse model and background used. Unlike CSF1R-ALSP patients, this mouse model was found to have increased microglial density with CSF1R heterozygous knockout, instead of depletion, suggesting active microgliosis contributing to the loss of myelin observed. [37]. Additionally, recent work by Stables et al. (BioRxiv preprint) has shown that pathophysiological effects in $CSF1R^{+/-}$ mice are strain and CX3CR1-function dependent, as disruption of CX3CR1 results in altered microglial function. That said, since TREM2 or DAP12 knockout in mice are unable to model the cardinal features of a related microgliopathy, Nasu-Hakola disease [45], it appears regardless of the specific disease, existing mouse models do not adequately or faithfully recapitulate many of the characteristics of human microgliopathies.

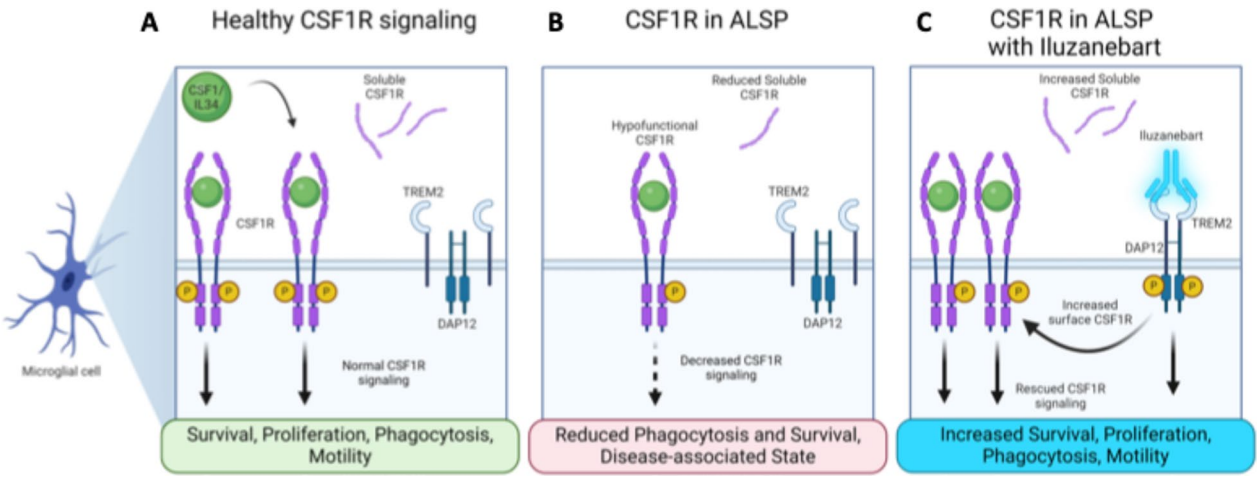

Fig. 11 Iluzanebart Proposed Mechanism of Action. **A** Healthy CSF1R signaling. Under normal conditions, ligand binding to CSF1R induces homodimerization and triggers transphosphorylation and activation of the CSF1R intracellular kinase domains, recruiting Src kinase and triggers downstream mediators such as SYK and transmembrane adapter protein DAP12, promoting microglia survival, proliferation, phagocytosis, and motility. Ligand binding to and activation of TREM2 also triggers the same intracellular signaling pathways through pSYK and through the DAP12 adapter protein. **B Dysfunctional CSF1R in CSF1R-ALSP.** When CSF1R receptors are dysfunctional due to genetic mutations, signaling through microglia health-promoting pathways is reduced (**C) Treatment of CSF1R-ALSP with iluzanebart.** Iluzanebart binds with high affinity to the extracellular domain of two TREM2 molecules, sequestering them in an active, dimerized state and activating microglia health-promoting downstream signaling to compensate for lost CSF1R signaling as well as increasing signaling through an increase in the amount of CSF1 receptors at the cell surface

Finally, iluzanebart offers a novel approach to TREM2 agonism via binding to a different region of the TREM2 receptor, resulting in the lack of receptor shedding inhibition, unlike other antibodies in development for Alzheimer's disease [44]. Alternatively, those findings could be explained by a compensatory increase in CSF1R signaling despite the underlying haplo-insufficient state caused by the potential liberation of DAP12 in a TREM2 KO model, potentially leading to a counterintuitive increase of CSF1R signaling, as CSF1R is able to signal through DAP12, in addition to signaling through autophosphorylation.

Ultimately, iluzanebart rescued multiple in vitro models of CSF1R-ALSP, in multiple human myeloid cell types. Importantly, iluzanebart was able to restore CSF1R surface levels on microglia and this resulted in increased pathway activation, the primary causal microglial deficit in CSF1R-ALSP. Our results are consistent with the hypothesis that TREM2 activation can compensate for CSF1R loss of function. Taken together, these data support the continued clinical development of iluzanebart as a therapeutic for CSF1R-ALSP.

Materials and methods

Iluzanebart

Iluzanebart is a human monoclonal IgG1 hTREM2 antibody, possessing a modified Fc domain to minimize effector function, formulated for intravenous (IV) administration. Iluzanebart is has been evaluated for safety and tolerability in a Phase 1 SAD/MAD trial in healthy volunteers. A Phase 2 proof-of-concept trial in patients with CSF1R-ALSP was initiated in December of 2022 (IGNITE, NCT05677659).

Purified iluzanebart and Fc-modified IgG1 used in these studies were produced by Thermo Fisher Scientific from plasmid transfection of ExpiCHO cells. Antibodies were subsequently purified by 2-step affinity purification and validated to be endotoxin free.

Reagents and antibodies

R&D anti-mouse/anti-rat antibody (#MAB17291), R&D Systems] anti-human TREM1 antibody (#MAB1278), Concanavalin A (Sigma, #C2010), PLX5622 (MedChem Express, #50-196-9292), IL4 (Peprotech #200-04).

HEK293T-hTREM2/1 cell line culture

HEK-293T cells were engineered to express human TREM2 and DAP12 (HEK293T-hTREM2 cells, Amgen). Mouse, rat, or cynomolgus macaque TREM2 and DAP12 (HEK293T-m/r/cTREM2 cell lines) were also generated by Amgen. Cells were maintained in growth media containing: DMEM-F12, 10% heat inactivated FBS (Fetal Bovine Serum), 1 × Pen-Strep, 1 × Glutamax, and 0.1 mg/mL Zeocin. Cells were used between passages 7 and 18 and maintained at below 80% confluence.

Iluzanebart potency assays in HEK cells

HEK-h/c/m/rTREM2 or TREM1 cells were plated at 14,000 cells per well in a 384-well plate, in 25 µL of complete growth media and incubated at 37 ℃, 5% CO2, for 20–24 h. Growth media was removed and 25 µL of iluzanebart, matched IgG, or positive control antibody in assay buffer were added to cells. Cells were incubated for 45 min at room temperature. Levels of SYK phosphorylation were measured using a commercial AlphaLISA reagent kit (Revvity, #ALSU-PSYK-A500). After 45 min, the assay buffer was removed and 10 µL of lysis buffer was added. Plates were then shaken for 20 min at 350 RPM at room temperature and AlphaLISA reagents were added to the lysate, according to manufacturer's instructions. Fluorescence intensity was measured using a Revvity Envision plate reader and was used to generate a standard curve. Curve fitting was performed using Prism v9 software, log(agonist) vs response – variable slope (four parameters), and EC50 was calculated from the curve fit.

hMDM cell preparation

Peripheral blood mononuclear cells (PBMCs) were isolated from fresh whole blood from human donors (Lonza #4W-270). CD14 + monocytes were isolated using positive magnetic selection according to manufacturer's instructions (Miltenyi #130–050-201). Cells were resuspended in culture media containing RPMI-1640 (Gibco #72400047), 10% heat inactivated FBS (Fetal Bovine Serum: Thermo #12484–028), Pen-Strep (Gibco #15140–122), Non-Essential Amino Acids (Gibco #111400050), Sodium Pyruvate (Gibco #11360070), 50 ng/mL human CSF1 (Thermo-Fisher #RP8643), and 10 ng/mL human IL4 (PeproTech #200–04).

hMDM CSF1 withdrawal assays

Isolated CD14 + cells were plated in 60 mm Up Cell low-adhesion plates (Nunc #174,901) and incubated in culture media for 48 h. After 48 h, cells were harvested and plated at 25,000 cells per well in 96 well cell culture plates (Corning #3997) coated with either 10 µg/mL iluzanebart or isotype control and incubated in a humidified incubator at 37 ℃ with 5% CO_2 for 72 h. Plates were prepared the day of cell plating by diluting antibodies to specified concentrations in PBS (Gibco #10010023) and incubating at 37 ℃ for 2 h. Plates were washed three times with PBS prior to cell plating.

For determination of caspase activity, cells were incubated with caspase 3/7 green dye (Sartorius #4440) and monitored every two hours using an IncuCyte S3 analyzer. Caspase 3/7 positive counts per field of view were calculated using IncuCyte software, and significance was determined in Graphpad Prism by Ordinary One-Way ANOVA, with correction for multiple comparisons. To quantify cell morphology, cells were monitored concurrently with caspase activity every two hours during incubation. Confluence levels were determined using the IncuCyte software, and normalized to CSF1 at 50 ng/mL, considered normal culture conditions. Cell viability was measured using Cell Titer Glo 2.0, (Promega, #G9241) according to manufacturer's instructions.

hMDM iCSF1R treatment assays

CD14 + cells were plated as described above for the CSF1 withdrawal experiments. After replating cells on iluzanebart or matching isotype control coated plates, iCSF1R (PLX5622; MedChem Express #HY-114153) was resuspended in DMSO diluted in culture media and added to cells to a final concentration of 1 µM, with a final DMSO concentration of 0.5%. Plates were incubated in a humidified incubator at 37C, 5% CO2 for an additional 96 h. During incubation cells were monitored every twenty-four hours using an Incucyte S3 analyzer. Confluence was measured using IncuCyte software, while area and eccentricity (cell shape) were measured using the "Cell by Cell" analysis. Cell viability was measured using CellTiter Glo 2.0 as described above in the CSF1 withdrawal experiments.

iMGL cell line cultures

Human iPS derived microglia were purchased from FujiFilm Cellular Dynamics (#C1110). Cells were thawed and incubated at 37 ℃, 5% CO_2 in a humidified incubator on Matrigel coated 6-well plates (Corning Biocoat, # 354,671) for three days, at a density of 500,000 cells per well in 2.5 mL of vendor supplied complete media containing growth factors. One day after plating, 1 mL of complete media containing IL4 was added to the cells, to a final concentration of 10 ng/mL. Cells were incubated an additional two days before plating for assays.

iMGL pSYK assay

After three days of incubation in 6 well plates, iMGLs were removed by gentle pipetting, centrifuged, resuspended in complete media, and replated into Sartorius ImageLock 96-well plates (# BA-04485) at a density of 15,000 cells/well. Iluzanebart or its matched IgG1 isotype control was diluted at half-log increments in culture media and added to cells. For Concanavalin A experiments, iMGL or TREM2 -/- microglia (Fujifilm #C1136) were plated as above. Concanavalin A was serially diluted in complete media and added to cells. Cells were incubated at 37 ℃, 5% CO_2 for 5 min. Media was then removed, and 25 µL lysis buffer was added into each well.

Assay plates were frozen immediately at – 80 ℃ overnight to lyse the cells. Lysates were subsequently used in the pSYK AlphaLISA assay according to manufacturer's protocol (Revvity #ALSU-PSYK-A10K). Fluorescence intensity was measured using SpectraMax i3X plate reader (Molecular Devices), and percent of control was calculated as % of IgG1 control raw signal. Curve fitting was performed using Graphpad Prism v9.2 software, with a log(agonist) vs response – variable slope (four parameters) curve fit, and EC50s and were calculated from this curve fit.

iMGL iCSF1R assay

Prior to plating iMGL, plates were coated as above with either iluzanebart or its matched IgG1 control at 75 μg/mL. Cells were plated at 15,000 cells per well in 96 well plates in complete media, and after 24 h, iCSF1R or DMSO (Vehicle Control) was added to the plate to bring the final concentration to 150 nM in 0.01% DMSO. During incubation, a subset of plates received caspase 3/7 dye (Sartorius, 1:1000 dilution). Caspase 3/7 labeled plates were then incubated in the IncuCyte SX3 and imaged every 6 h for a total of 48 h. After 48 h, plates were allowed to recover to room temperature and a CellTiter Glo 2.0 assay was performed according to manufacturer's instructions. Luminescence was then measured using the SpectraMax i3X plate reader (Molecular Devices). Data was quantified and analyzed in Graphpad Prism v9.2 software. Images from IncuCyte were quantified using the same analysis on the IncuCyte 2020B software to measure confluence, morphology (eccentricity, via Cell-by-Cell module), and caspase 3/7 dye signal. Experiments were repeated three more times for four independent experiments.

iMGL CSF1R flow cytometry

iPSC derived microglia were plated on 24 well plates coated with iluzanebart or its matched IgG control (as previously described) for 24 h. Cells were harvested by scraping and stained with LIVE/DEAD™ Fixable Violet Dead Cell Stain (1:1000, ThermoFisher) and Human TruStain FcX (1:20, Biolegend) for 15 min at room temperature. Cells were fixed with 2% Paraformaldehyde for 15 min at room temperature, followed by staining with a cocktail containing CSF1R and CD45 antibodies, or isotype control IgG1 (1:50, Biolegend) and Brilliant Stain Buffer (ThermoFisher). Internal expression was assessed in a portion of the cells by including eBioscience Permeabilization Buffer (ThermoFisher) during staining at room temperature for 30–60 min. Surface expression was probed by staining on ice for 30–60 min. Cells were analyzed by flow cytometry using the Attune NxT Flow Cytometer and FlowJo™ v10.10.0 Software (BD Life Sciences).

iMGL CSF1 withdrawal assay

After 3 days incubation in 6 well plates, iMGL were resuspended in one of two media: Complete Media or Withdrawal Media (Complete Media without a supplement that contained CSF1 and IL34). Prior to plating of cells, plates were coated as previously described with either iluzanebart or a matched IgG1 control at 75 μg/mL to ensure complete coating of the plates. Cells were plated at 15,000 cells per well in each media, in 96 well plates. During incubation, a subset of plates received caspase 3/7 dye (Sartorius, 1:1000 dilution). Caspase 3/7 labeled cells were then incubated in the IncuCyte SX3 and imaged every 6 h for a total of 48 h. Plates without caspase dye were incubated in a humidified 5% CO_2 incubator, at 37C for 48 h. After 48 h, plates were allowed to recover to room temperature and a CellTiter Glo 2.0 assay was performed according to manufacturer's protocol. Luminescence was then measured using the SpectraMax i3X plate reader (Molecular Devices). Data was quantified and analyzed in Graphpad Prism v9.2 software. Images from IncuCyte were quantified using the same analysis on the IncuCyte 2020B software to measure confluence, morphology (eccentricity, via Cell-by-Cell module, run according to manufacturer's instructions, with eccentricity being defined as the degree of lack of roundness to the cell), and caspase 3/7 dye signal. Experiments were repeated three more times for four independent experiments.

sTREM2 and sCSF1R assays

iMGL were plated as previously described at 15,000 cells per well in 96 well plates coated with iluzanebart or its matched IgG1 control in dose response. Plates were incubated for 24 h in a humidified 5% CO_2 incubator, at 37 ℃. After 24 h, 50 μL of cell culture supernatant was removed and stored in polypropylene plates at –80 ℃ until ELISAs could be performed. CellTiterGlo 2.0 assay was immediately performed on the cells to normalize for cell numbers, according to manufacturer's instructions. Both human TREM2 and human CSF1R ELISA assays (Abcam #ab224881 and #ab230940) were performed according to manufacturer's protocol. Data was then entered into Prism Graphpad for visualization and statistical analysis.

Human iPSC derived microglia with a CSF1R-ALSP relevant mutation

Heterozygous I794T ($I794T^{+/-}$) iPSC were generated using CRISPR technology by Synthego, from parent line ASE-9211 (Applied Stem Cell). All microglial differentiation work was performed by Axol Biosciences. iPS cells

were differentiated to monocyte-like cells using Axol's proprietary protocol, and cell quality was verified by flow cytometry for 6 different markers. Monocyte-like cells were plated at 30,000 cells per well on 25 µg/mL iluzanebart or IgG1 coated plates (prepared as previously described) in media containing reduced levels of IL34 and CSF2. Plate coating concentrations were chosen to be lower compared to hMDM and iMGL rescue experiments, to determine minimal concentration required for rescue. Fresh media was added on day 4 of culture. On day 7 of culture, cells were assayed for viability using CellTiter Glo (Promega) and for phospho-CSF1R (R&D Systems #DYC3268) or levels of CSF1R in the media or levels of total CSF1R in cell lysates (R&D Systems #DY329) according to manufacturer's instructions. Data is shown normalized to cell number at the end of the experiment as determined by Incucyte's cell counting analysis software.

hTREM2 transgenic mouse generation

hTREM2-CV transgenic mice were originally generated by Marco Colonna [37] and licensed from Washington University by Vigil Neuroscience. Briefly, transgenic mice were generated using the human TREM2 CTD-2210D2 bacterial artificial chromosome (BAC) clone which includes the entire coding region and endogenous regulatory elements. The BAC transgene was injected into the nucleus of fertilized eggs from C57BL/6 mice, and hTREM2-CV founders were selected. Founders were back-crossed to mouse TREM2 -/-, C57BL/6 animals to generate a human-specific TREM2 expressing line. Mice were housed at Charles River Laboratories under pathogen free conditions. Genotyping for the human TREM2 transgene was performed by Transnetyx using RT-PCR, and hTREM2-CV or TREM2 -/- mice were selected for in vivo studies.

In vivo *iluzanebart treatment protocol*

Transgenic mice were administered intraperitoneally with iluzanebart (1, 3, 10, 30, 100 and 200 mg/kg) or isotype control IgG1 (100 mg/kg). Plasma samples were serially collected for the determination of iluzanebart concentrations at 1, 2, 4, 8, and 24 h following single administration. At 24 h post-dose, animals were transcardially perfused with cold PBS followed by removal of the brain and sub-dissection into hippocampus, cortex, and cerebellum for the analysis of RNAseq and cytokines and the determination of iluzanebart concentrations, allowing for multiple PK/PD analyses from the same mouse sample. Samples were stored at -80 ℃ until processed for analysis.

Determination of iluzanebart concentrations in plasma and cerebellum samples

For cerebellum sample preparation, glass beads and tris lysis buffer containing protease and phosphatase inhibitors at a ratio of 1:4 (weight: volume) were added to the tissue in a microcentrifuge. After homogenization at 4 °C with the Fastprep 24 homogenizer (2 × 60 s cycles; Speed: 6.0), samples were centrifuged at 13,000 rpm for 10 min at 4 °C. The supernatant was stored at −80 °C until analysis. Iluzanebart concentrations in mouse plasma and brain homogenate were assessed for binding to the antibodies provided in the commercial human IgG MSD kit. Data was processed using Workbench 4.0® and quantified using a calibration curve of iluzanebart standards.

Brain hippocampal tissue RNAseq analysis

RNA extraction, library preparation, sequencing, and analysis were conducted at Azenta Life Sciences (South Plainfield, NJ, USA). Total RNA was extracted from Frozen Tissues samples using Qiagen RNeasy Plus Universal Mini Kit following manufacturer's instructions (Qiagen, Hilden, Germany). RNA samples were quantified using Qubit 2.0 Fluorometer (ThermoFisher Scientific, Waltham, MA, USA) and RNA integrity was checked with 4200 TapeStation (Agilent Technologies, Palo Alto, CA, USA). RNA sequencing library was prepared using the NEBNext Ultra II RNA Library Prep Kit for Illumina using manufacturer's instructions (New England Biolabs, Ipswich, MA, USA). Briefly, mRNA was initially enriched with Oligo(dT) beads. Enriched mRNAs were fragmented for 15 min at 94 °C. First strand and second strand cDNA are subsequently synthesized. cDNA fragments are end repaired and adenylated at 3'ends, and universal adapters are ligated to cDNA fragments, followed by index addition and library enrichment by PCR with limited cycles. The sequencing library was validated using the Agilent Tapestation 4200 (Agilent Technologies, Palo Alto, CA, USA), and quantified using Qubit 2.0 Fluorometer (ThermoFisher Scientific, Waltham, MA, USA) as well as by quantitative PCR (KAPA Biosystems, Wilmington, MA, USA). The sequencing libraries were multiplexed and clustered onto a flowcell. After clustering, the flowcell was loaded onto the Illumina HiSeq 3000/4000 or equivalent instrument according to manufacturer's instructions. The samples were sequenced using a 2 × 150 bp Paired End (PE) configuration. Image analysis and base calling were conducted by the HiSeq Control Software. Raw sequence data generated from Illumina was converted into fastq files and de-multiplexed using Illumina bcl2fastq 2.20 software. One mismatch was allowed for index sequence identification.

Sequence reads were trimmed to remove possible adapter sequences and nucleotides with inferior

quality using Trimmomatic v.0.36. The trimmed reads were mapped to the Mus musculus GRCm38 reference genome available on ENSEMBL using the STAR aligner v.2.5.2b. The STAR aligner is a splice aligner that detects splice junctions and incorporates them to help align the entire read sequences. Unique gene hit counts were calculated by using feature Counts from the Subread package v.1.5.2. Only unique reads that fell within exon regions were counted. Using DESeq2, a comparison of gene expression between the groups of samples was performed. The Wald test was used to generate p-values and Log2 fold changes. Genes with an adjusted p-value < 0.05 were called as differentially expressed for each comparison.

In vivo *cytokine analyses*

Chemokine concentrations were quantified using a commercial V-PLEX Cytokine Panel 1 (mouse) Kit from Meso Scale Discovery (Catalog # K15245D). Briefly, samples were treated as outlined in the provided manufacturer protocol. Right cortices were homogenized in a solution of Tris Lysis Buffer containing Protease and Phosphatase Inhibitor (4 mL for each gram of brain tissue) using Bead Ruptor Elite bead mill homogenizer and the resulting brain homogenates were subsequently diluted twofold with MSD assay Diluent 41® prior to addition to the plate and analysis. Pre-coated Cytokine Panel 1 mouse plate was washed 3 times with 150 µL / well of PBS + 0.05% Tween® 20 buffer. After washing, diluted brain homogenates samples (50 µL) along with calibrator was loaded on the plate and allowed to incubate for 2 h with shaking at room temperature. Next, the plate was washed 3 times and incubated with 25 µL of detection antibody solution for 2 h while shaking at room temperature. After washing of the plate, MSD proprietary read buffer was added, and the plate was read by an MSD QuickPlex SQ 120 system. Data was processed using Workbench 4.0® and quantified using calibrators run on the same plate as the samples.

In vivo *proliferation assay*

Equal numbers of adult male and female hTREM2-CV mice were administered intraperitoneally with 200 mg/kg iluzanebart, 200 mg/kg isotype control IgG1, or an equal volume of saline. At 48 h post-dose, animals were anesthetized and transcardially perfused with cold HBSS followed by perfusion with cold fixation buffer (Biolegend #420801). Whole brains, excluding cerebellum, were removed and placed in paraformaldehyde quench solution (HBSS, 5 mM HEPES, 250 mM Tris, 250 mM Glycine) before being incubated in digestion buffer (RPMI-1640, 5 mM HEPES, 800 U/mL Collagenase IV (Worthington # LS004189)) at 37C for no more than 4 h. Samples were then centrifuged, and cold FACS buffer (HBSS, 5 mM HEPES, 0.5% BSA, 2 mM EDTA) was added to stop digestion. This was followed by an additional centrifugation in 20% BSA (Sigma #126625) to remove myelin. Pellets were resuspended in 0.2 M acetic acid in 0.9% saline for 15 min, before resuspending in blocking buffer (HBSS, 5 mM HEPES, 20% Ovalbumin (Sigma #A5503), 20% Mouse Serum (Sigma #M5905) for 15 min. Samples underwent an additional centrifugation step and were resuspended in 2% paraformaldehyde to complete fixation of cells. Samples were then placed in 96 well v- bottom plates (USA Scientific #18339600), 100 µL per well and 10 samples per brain. 100 µL FACS buffer was added to wash, and after an additional centrifugation, supernatant was removed and pellets were resuspended in antibody panels (Biolegend: mCD45, clone 30-F11; mCD68, clone FA-11; mKi-67, clone 16A8; mCSF1R, clone W19330C; human IgG1; clone M1310G05, and DRAQ5) and Brilliant Violet Stain Buffer (BD 563794) in 1 × permeabilization buffer (Invitrogen #00-8333-56) and allowed to stain at room temperature for 30 min. Cells were analyzed by flow cytometry using the Attune NxT Flow Cytometer and FlowJo™ v10.10.0 Software (BD Life Sciences). Tissue samples from mice without detectable drug present, as determined by anti-human IgG positive microglia, were excluded from the analysis.

Supplementary Information

The online version contains supplementary material available at https://doi.org/10.1186/s12974-025-03346-1.

Additional file 1: All adjusted p-value <0.05 differentially expressed genes by bulk RNAseq on hippocampus of hTREM2 mice treated with iluzanebart for 24 h.

Additional file 2: Figure 1. Epitope Mapping of Binding of Iluzanebart to TREM2 by HDX-MS. (A) Heat map depicting results of hydrogen/deuterium exchange (HDX) mass spectrometry (MS) for TREM2 + iluzanebart. Blue indicates areas of antibody binding; three timepoints of incubation are shown (0.25 min, 1 min, and 60 min). (B) Three-dimensional depiction of antibody binding sites on the TREM2 protein after 1 minute of incubation. Figure 2. TREM2 receptor binding SPR assay. Surface plasma resonance (SPR) demonstrating iluzanebart binding interaction with ligand TREM2 (n=3). Figure 3. Iluzanebart does not activate mouse or rat TREM2. (A) Mouse TREM2-HEK. In HEK293T cells expressing mouse TREM2 and DAP12, pDAP12 in response to iluzanebart for 45 minutes was analyzed, resulting in no activation by iluzanebart (n = 2 independent experiments), while a control mouse TREM2 agonist antibody worked as expected (B) Rat TREM2-HEK. Similarly, in rat HEK293T cell line, iluzanebart showed no ability to activate SYK (n=3 independent experiments), while a rat TREM2 agonist behaved as expected. Figure 4. Pharmacokinetic analysis of iluzanebart in hTREM2 mice Terminal iluzanebart brain concentrations and corresponding fold exposures over in vitro sCSF1R EC_{50} and sTREM2 IC_{50} pharmacologically align with on-target TREM2 agonism. Values are means +/- standard deviation, n=4-6 mice per group. (A) Plasma concentrations of iluzanebart. 100 and 200 mg/kg were above limit of quantitation and were excluded. Figure 5. Presence of human IgG in mouse brain post 48-hour dosing. To ensure that only mice with detectable levels of iluzanebart or IgG control were included in the analysis, samples were analyzed for levels of human IgG. Mice without detectable levels of IgG were

excluded from the iluzanebart and IgG control groups. Two mice with no detectable human IgG from IgG control group and from the iluzanebart treatment group were excluded (blue circle). Saline treated samples (grey) showed no detectable human IgG, as expected. Additionally, levels of Ki67 positive microglia positively correlated with levels of anti-human IgG positive microglia, with a pearson correlation coefficient r of 0.89.

Acknowledgements
We would like to thank David Wallbank at Axol Bioscience for his assistance in differentiation of wildtype and I794T$^{+/-}$ iPSC to microglia, and performing all experiments utilizing these differentiated cells . We would also like to thank Christine Kirady, Marine Diennet, Yael Mamane, Jianhong Liu, Emilie Gravel, and Zuomei Li at Nuchem Sciences for their assistance in performing SYK phosphorylation assays. NuChem Sciences performed all work with HEK cell lines, as well as the pSYK assay in hMDMs. Daria Tchessalova performed the pSYK assay in iMGL, as well as in the TREM2-/- iMGL.

Author contributions
A.R. performed CSF1Ri and CSF1 withdrawal experiments in hMDM. A.R. and E.W. performed the CSF1R surface level experiments in iMGL. F.G. performed sTREM2 assay, sCSF1R assay, PLX5622 treatments, and CSF1 withdrawal experiments in iMGL. The in-life portion of all hTREM2 mice work was performed by Charles River Laboratories. B.D. managed iluzanebart in vivo studies in conjunction with Charles River Labs and Azenta sciences. E.T. oversaw pharmacokinetic studies. B.P. managed all SPR (Surface Plasma Resonance) and HDX work in conjunction with Viva Sciences. Experimental concept, design and management by K.L., B.L., R.F., D.G., and C.M. Epidemiological information provided by D.M. Pharmacokinetic modeling and analysis provided by L.H. and F.G. Manuscript and figures generated by K.L. and A.R. Figure 11 generated using Biorender by A.R.

Funding
This work was entirely funded by Vigil Neuroscience and received no specific grant from any funding agency in the public, commercial, or not-for-profit sectors.

Data availability
No datasets were generated or analysed during the current study.

Declarations

Ethics approval and consent to participate
These studies followed national and institutional guidelines for humane animal treatment, with protocols reviewed and approved by the Charles River Laboratories Institutional Animal Care and Use Committee (IACUC).

Competing interests
The authors declare no competing interests.

Author details
[1]Vigil Neuroscience Inc, 100 Forge Road, Watertown, MA 02472, USA. [2]Vigil Neuroscience Inc. (Ret), 100 Forge Road, Watertown, MA 02472, USA. [3]Eikonizo Therapeutics, Inc, 245 Main St, Cambridge, MA 02142, USA.

Received: 30 September 2024 Accepted: 14 January 2025
Published online: 31 January 2025

References

1. Konno T, Yoshida K, Mizuno T, Kawarai T, Tada M, Nozaki H, et al. Clinical and genetic characterization of adult-onset leukoencephalopathy with axonal spheroids and pigmented glia associated with CSF1R mutation. Eur J Neurol. 2016;24(1):37–45.
2. Ikeuchi T, Mezaki N, Miura T. Cognitive dysfunction and symptoms of movement disorders in adult-onset leukoencephalopathy with axonal spheroids and pigmented glia. Parkinsonism Relat Disord. 2018;46:39–41.
3. Wade C, Runeckles K, Chataway J, Houlden H, Lynch DS. CSF1R -related disorder : prevalence of CSF1R variants and their clinical significance in the UK population. Neurol Genet. 2024. https://doi.org/10.1212/NXG.0000000000200179.
4. Papapetropoulos S, Gelfand JM, Konno T, Ikeuchi T, Pontius A, Meier A, et al. Clinical presentation and diagnosis of adult-onset leukoencephalopathy with axonal spheroids and pigmented glia: a literature analysis of case studies. Front Neurol. 2024;11:15.
5. Konno T, Kasanuki K, Ikeuchi T, Dickson DW, Wszolek ZK. CSF1R -related leukoencephalopathy: a major player in primary microgliopathies. Neurology. 2018;91(24):1092–104.
6. Du Q, Chen H, Shi Z, Zhang Y, Wang J, Zhou H. A novel mutation in the CSF1R gene causes hereditary diffuse leukoencephalopathy with axonal spheroids. Neurol Sci. 2019;40(6):1287–90.
7. Leng C, Lu L, Wang G, Zhang Y, Xu Y, Lin X, et al. A novel dominant-negative mutation of the CSF1R gene causes adult-onset leukoencephalopathy with axonal spheroids and pigmented glia. Am J Transl Res. 2019;11(9):6093–101.
8. Rosa R, Matt B, Nicholson Alexandra M, Rutherford Nicola J, NiCole F, Alexandra S-O, et al. Mutations in the colony stimulating factor 1 receptor (CSF1R) gene cause hereditary diffuse leukoencephalopathy with spheroids. Nat Gen. 2011;2:200–5.
9. Kraya T, Quandt D, Pfirrmann T, Kindermann A, Lampe L, Schroeter ML, et al. Functional characterization of a novel CSF1R mutation causing hereditary diffuse leukoencephalopathy with spheroids. Mol Genet Genomic Med. 2019. https://doi.org/10.1002/mgg3.595.
10. Stanley ER, Chitu V. CSF-1 receptor signaling in myeloid cells. Cold Spring Harb Perspect Biol. 2014;6(6):A21857.
11. Erblich B, Zhu L, Etgen AM, Dobrenis K, Pollard JW. Absence of colony stimulation factor-1 receptor results in loss of microglia, disrupted brain development and olfactory deficits. PLoS ONE. 2011;6(10):E26317.
12. Kempthorne L, Yoon H, Madore C, Smith S, Wszolek ZK, Rademakers R, et al. Loss of homeostatic microglial phenotype in CSF1R-related Leukoencephalopathy. Acta Neuropathol Commun. 2020;8(1):72.
13. Oosterhof N, Kuil LE, van der Linde HC, Burm SM, Berdowski W, van Ijcken WFJ, et al. Colony-stimulating factor 1 receptor (CSF1R) regulates microglia density and distribution, but not microglia differentiation in vivo. Cell Rep. 2018;24(5):1203–17.
14. Tada M, Konno T, Tada M, Tezuka T, Miura T, Mezaki N, et al. Characteristic microglial features in patients with hereditary diffuse leukoencephalopathy with spheroids. Ann Neurol. 2016;80(4):554–65.
15 Deczkowska A, Weiner A, Amit I. The physiology, pathology, and potential therapeutic applications of the TREM2 signaling pathway. Cell. 2020;181(6):1207–17.
16. Konishi H, Kiyama H. Microglial TREM2/DAP12 signaling: a double-edged sword in neural diseases. Front Cell Neurosci. 2018;12:206.
17 Humphrey MB, Xing J, Titus A. The TREM2-DAP12 signaling pathway in Nasu-Hakola disease: a molecular genetics perspective. Res Rep Biochem. 2015;2015:89–100.
18. Keren-Shaul S, Weiner M-N, Dvir-Szternfeld U, et al. A unique microglia type associated with restricting development of Alzheimer's disease. Cell. 2017;169(7):1276–90.
19. Zheng H, Jia L, Liu C-C, Rong Z, Zhong L, Yang L, et al. TREM2 promotes microglial survival by activating Wnt/β-catenin pathway. J Neurosci. 2017;37(7):1772–84.
20. Wang S, Mustafa M, Yuede CM, Salazar SV, Kong P, Long H, et al. Anti-human TREM2 induces microglia proliferation and reduces pathology in an Alzheimer's disease model. J Exp Med. 2020. https://doi.org/10.1084/jem.20200785.
21. Korvatska O, Leverenz JB, Jayadev S, McMillan P, Kurtz I, Guo X, et al. R47H variant of TREM2 associated with Alzheimer disease in a large late-onset family: clinical, genetic, and neuropathological study. JAMA Neurol. 2015;72(8):920–7.
22. Ruiz A. Assessing the role of the TREM2 p.R47H variant as a risk factor for Alzheimer's disease and frontotemporal dementia. Neurobiol Aging. 2014;35(2):225–46.
23. Marco C. TREMs in the immune system and beyond. Nat Rev Immunol. 2003;3(6):445–53.
24. Schlepckow K, Monroe KM, Kleinberger G, Cantuti-Castelvetri L, Parhizkar S, Xia D, et al. Enhancing protective microglial activities with a dual

function TREM2 antibody to the stalk region. EMBO Mol Med. 2020. https://doi.org/10.15252/emmm.201911227.
25. Ellwanger DC, Wang S, Brioschi S, Shao Z, Green L, Case R, et al. Prior activation state shapes the microglia response to antihuman TREM2 in a mouse model of Alzheimer's disease. Proc Natl Acad Sci U S A. 2021;118(3):E2017742118.
26. Stanley ER, Chitu V. CSF-1 receptor signaling in myeloid cells. Cold Spring Harb Perspect Biol. 2014. https://doi.org/10.1101/cshperspect.a021857.
27. Takeuchi F, Taniguchi T, Maeda H, Fujii C, Takeuchi N, Yamamura H. The lectin concanavalin a stimulates a protein-tyrosine kinase p72^s^y^k in peripheral blood lymphocytes. Biochem Biophys Res Commun. 1993;194(1):91–6.
28. Wunderlich G, Kemmerling T, Neumann W. Sequential proteolytic processing of the triggering receptor expressed on myeloid cells-2 (TREM2) protein by ectodomain shedding and γ-secretase-dependent intramembranous cleavage*. J Biol Chem. 2013;288(46):33027–36.
29. Kleinberger G, Yamanishi Y, Suárez-Calvet M, Czirr E, Lohmann E, Cuyvers E, et al. TREM2 mutations implicated in neurodegeneration impair cell surface transport and phagocytosis. Sci Transl Med. 2014;6(243):243.
30. Thornton P, Sevalle J, Deery MJ, Fraser G, Zhou Y, Ståhl S, et al. TREM2 shedding by cleavage at the H157–S158 bond is accelerated for the Alzheimer's disease-associated H157Y variant. EMBO Mol Med. 2017;9(10):1366–78.
31. Halaas NB, Henjum K, Blennow K, Dakhil S, Idland A-V, Nilsson LN, et al. CSF sTREM2 and tau work together in predicting increased temporal lobe atrophy in older adults. Cereb Cortex. 2020;30(4):2295–306.
32. Ewers M, Franzmeier N, Suárez-Calvet M, Morenas-Rodriguez E, Caballero MAA, Kleinberger G, et al. Increased soluble TREM2 in cerebrospinal fluid is associated with reduced cognitive and clinical decline in Alzheimer's disease. Sci Transl Med. 2019;11(507):6221.
33. Elizabeth S, Paul S, Lindsay H, Joshua C, Jiazhong Z, Elizabeth B, et al. Sustained microglial depletion with CSF1R inhibitor impairs parenchymal plaque development in an Alzheimer's disease model. Nat Commun. 2019;10(1):3758.
34. Mun SH, Park PSU, Park-Min K-H. The M-CSF receptor in osteoclasts and beyond. Exp Mol Med. 2020;52(8):1239–54.
35. Rajagovindan R, Matys B, Finger E, Gelfand JM, Isaacson S, Köhler W, et al. A Prospective natural history study of patients with adult-onset leukoencephalopathy with axonal spheroids and pigmented glia (ALSP). Neurology. 2023. https://doi.org/10.1212/WNL.0000000000203073.
36. Haenseler W, Sansom SN, Buchrieser J, Newey SE, Moore CS, Nicholls FJ, et al. A highly efficient human pluripotent stem cell microglia model displays a neuronal-co-culture-specific expression profile and inflammatory response. Stem Cell Reports. 2017;8(6):1727–42.
37. Song WM, Joshita S, Zhou Y, Ulland TK, Gilfillan S, Colonna M. Humanized TREM2 mice reveal microglia-intrinsic and -extrinsic effects of R47H polymorphism. J Exp Med. 2018;215(3):745–60.
38. Gratuze M, Leyns CEG, Sauerbeck AD, St-Pierre M-K, Xiong M, Kim N, et al. Impact of TREM2R47H variant on tau pathology–induced gliosis and neurodegeneration. J Clin Investig. 2020;130(9):4954–68.
39. Deczkowska K-S, Weiner C, Schwartz A. Disease-associated microglia: a universal immune sensor of neurodegeneration. Cell. 2018;173(5):1073–81.
40. Chitu G, Gulinello B, Patil B, et al. Phenotypic characterization of a Csf1r haploinsufficient mouse model of adult-onset leukodystrophy with axonal spheroids and pigmented glia (ALSP). Neurobiol Dis. 2015;74:219–28.
41. Arreola MA, Soni N, Crapser JD, Hohsfield LA, Elmore MRP, Matheos DP, et al. Microglial dyshomeostasis drives perineuronal net and synaptic loss in a CSF1R+/– mouse model of ALSP, which can be rescued via CSF1R inhibitors. Sci Adv. 2021;7:35.
42. Patkar C, Teakle K, Bush P, et al. Analysis of homozygous and heterozygous Csf1r knockout in the rat as a model for understanding microglial function in brain development and the impacts of human CSF1R mutations. Neurobiol Dis. 2021. https://doi.org/10.1016/j.nbd.2021.105268.
43. Chadarevian JP, Hasselmann J, Lahian A, Capocchi JK, Escobar A, Lim TE, et al. Therapeutic potential of human microglia transplantation in a chimeric model of CSF1R-related leukoencephalopathy. Neuron. 2024;112(16):2686–707.
44. Kariolis MS, et al. Brain delivery of therapeutic proteins using an Fc fragment blood-brain barrier transport vehicle in mice and monkeys. Sci Transl Med. 2020;12(545):1359.
45. Zhou Y, Tada M, Cai Z, Andhey PS, Swain A, Miller KR, Gilfillan S, Artyomov MN, Takao M, Kakita A, Colonna M. Human early-onset dementia caused by DAP12 deficiency reveals a unique signature of dysregulated microglia. Nat Immunol. 2023;24(3):545–557. https://doi.org/10.1038/s41590-022-01403-y. Epub 2023 Jan 19. Erratum in: Nat Immunol. 2023;24(3):558. https://doi.org/10.1038/s41590-023-01465-6.

Publisher's Note